The Outer Halo of the Milky Way as Probed by RR Lyr Variables from the Palomar Transient Facility [1]

Judith G. Cohen[2], Branimir Sesar[2,3], Sophianna Bahnolzer[4], Kevin He[2], Shrinivas R. Kulkarni[2], Thomas A. Prince[2], Eric Bellm[2,5], Russ R. Laher[6]

ABSTRACT

RR Lyr stars are ideal massless tracers that can be used to study the total mass and dark matter content of the outer halo of the Milky Way. This is because they are easy to find in the light curve databases of large stellar surveys and their distances can be determined with only knowledge of the light curve. We present here a sample of 112 RR Lyr beyond 50 kpc in the outer halo of the Milky Way, excluding the Sgr streams, for which we have obtained moderate resolution spectra with Deimos on the Keck 2 Telescope. Four of these have distances exceeding 100 kpc. These were selected from a much larger set of 447 candidate RR Lyr which were datamined using machine learning techniques applied to the light curves of variable stars in the Palomar Transient Facility database. The observed radial velocities taken at the phase of the variable corresponding to the time of observation were converted to systemic radial velocities in the Galactic standard of rest. From our sample of 112 RR Lyr we determine the radial velocity dispersion in the outer halo of the Milky Way to be $\sim$90 km s^{-1} at 50 kpc falling to about 65 km s^{-1} near 100 kpc once a small number of major outliers are removed. With reasonable estimates of the completeness of our sample of 447 candidates and assuming a spherical halo, we find that the stellar density in the outer halo declines as r^{-4}.

---

[1]Based in part on observations obtained at the W.M. Keck Observatory, which is operated jointly by the California Institute of Technology, the University of California, and the National Aeronautics and Space Administration.

[2]Division of Physics, Mathematics and Astronomy, California Institute of Technology, Pasadena, Ca., 91125, jlc@astro.caltech.edu, khe@caltech.edu, srk@astro.caltech.edu, prince@srl.caltech.edu, ebellm@astro.caltech.edu

[3]Max Planck Institute for Astronomy, Konigstuhl 17, D-69117, Heidelberg, Germany, bsesar@mpia.de

[4]535 Pontius Ave. N., Apt. 507, Seattle, WA, 98109, sophianna.banholzer@gmail.com

[5]Box 351580, University of Washington, Seattle, Washington, 98195,ecbellm@uw.edu

[6]Infrared Processing and Analysis Center, California Institute of Technology, Pasadena, Ca., 91125

Subject headings: stars: variables: RR Lyra – Galaxy halo — Galaxy: kinematics and dynamics

1. Introduction

We present initial results of a study of the outer halo of the Milky Way (henceforth MW) using a large sample of RR Lyr type ab (denoted as RRab) variables. RR Lyr are old low-mass pulsating stars with distinctive light curves, amplitudes at R of $\sim$0.5 to 1 mag, and periods of $\sim$0.4 to 0.8 days, which are unchanged on a timescale of years and in most cases decades or longer. These characteristics make them fairly easy to distinguish in a wide field, multi-epoch optical imaging survey if the survey cadence is suitable. Their most desirable characteristic is that they are standard candles. Accurate luminosities, which have only a small dependence on metallicity and period (see the discussion in §4), can be inferred directly from the light curves, and these stars, with $M_V \sim +0.6$ mag, are fairly luminous and hence can be detected at large distances.

There is a long history reaching back more than 30 years of efforts to calibrate the RR Lyr period-luminosity-metallicity relation, many of which use the Baade-Wesselink (Baade 1926; Wesselink 1969) infrared surface brightness technique to establish an accurate distance scale. Their subsequent use as distance indicators within the MW halo, primarily for globular clusters and distant halo stars, also has a long history, see, e.g. Longmore, Fernley & Jameson (1986), Cohen (1992), and many other early efforts. Early calibration efforts (see, e.g. Longmore, Fernley & Jameson 1990) demonstrated the advantages of using IR photometry rather than optical photometry, specifically lower amplitude of variation meaning that fewer epochs are required to determine a mean magnitude, hence a luminosity. Now with the Spitzer IRAC camera (Werner et al. 2004; Fazio et al. 2004) and the WISE all sky survey (Wright et al. 2010), highly accurate photometry on a stable space based platform enables even more precise distances for RR Lyr, with recent period-luminosity calibrations for the WISE bandpasses carried out by Madore et al. (2013) and by Klein et al. (2014). Furthermore, the HST-Fine Guidance Sensor cameras were used by Benedict et al. (2011) to determine trigonometric parallaxes to several of the nearest field RR Lyr, in principle providing a fundamental calibration for all these efforts. Sesar et al. (2017a) used the Tycho-GAIA Astrometric Solution (Michalik, Lindegren & Hobbs 2015) parallaxes of nearby RR Lyr from the GAIA Data Release 1 (GAIA collaboration 2016) to verify existing period–luminosity–metallicity relationships of previous studies, illustrating the potential for very high accuracy distances for RR Lyr stars with future GAIA releases.

Our survey for RR Lyr is focused on fundamental mode pulsators, i.e. RR Lyr type

ab. Type *c* RR Lyr stars, which are first overtone pulsators, comprise roughly 23% of the total RR Lyr population (Soszynski et al. 2016). They are systematically less luminous than RRab by about 0.25 mag and have shorter periods (Braga et al. 2015). RR Lyr type *c* can be distinguished from fundamental mode pulsators by their smoother, more sinusoidal light curves, but this makes their separation from contact binary systems more challenging.

We are now in an era of large digital imaging surveys, including the SDSS (York et al. 2000), the Palomar Transient Facility (Law et al 2009, Rau et al. 2009) and its successors, the Catalina Real-Time Transient Surveys (CRTS) (Djorgovski et al 2011), and the Pan-STARRS survey (Hodapp et al. 2004; Tonry et al. 2012), with LSST coming in the next decade. GAIA recently had its first data release as well (GAIA collaboration 2016), with more to follow in due course. These surveys, with their huge databases can, depending on their cadences and limiting magnitudes, be used to identify ever larger samples of ever more distant RR Lyr, continuing and expanding on much earlier efforts (see, e.g. Wetterer & McGraw 1996). Such samples enable studies of the outer halo of the Milky Way, as well as of streams and substructures therein. RR Lyr are particularly useful for isolating halo substructures as they stand out through their variability and blue color against the numerous foreground Galactic disk and inner halo stars; Sesar et al. (2012) and Sesar et al. (2013b) have utilized the Palomar Transient Facility (PTF) samples for this purpose.

Our survey for RR Lyr in the outer halo of the Galaxy carried out with the PTF begins at a heliocentric distance of 50 kpc and reaches out to distances of ∼110 kpc. Previous surveys of halo RR Lyr stars include Vivas et al. (2001), Keller et al. (2008), Miceli et al. (2008), Sesar et al. (2011), Sesar et al. (2013a) and Drake et al (2014), among others. Our survey presents a significant improvement over anything previously published in sample size and in precision of distances in the 50 to 100 kpc range. We present in this paper the radial velocity data obtained to date for these distant RR Lyr through moderate resolution spectroscopy at the Keck Observatory as well as a preliminary halo density distribution derived from our full RR Lyr sample.

An overview of the PTF is given in §2. The following sections briefly review how we derived our RR Lyr sample, then describe how we calculate distances from the light curve parameters. We then discuss our spectroscopic follow-up campaign at the Keck Observatory to measure radial velocities, and present v_r for 112 RR Lyr in the outer halo of the MW with heliocentric distances ranging from 50 to 109 kpc, and with median distance of 73 kpc, which we subsequently use to derive the velocity dispersion in the outer halo of the MW. Next we give a description of our preliminary halo density distribution derived from our full sample of 447 RR Lyr candidates. This is followed by a comparison of our results with the results of other recent studies of the outer halo of the MW, and a summary.

2. Overview of the Palomar Transient Facility

The PTF (Law et al 2009; Rau et al. 2009) (P.I. S. R. Kulkarni of Caltech) is a wide-area, two-band (g and R filters), deep (R ∼20.6 single-epoch, ∼23 mag co-added) survey aimed at systematic exploration of the optical transient sky. The PTF ran for three years, ending Dec. 31, 2012, then transitioned to the intermediate-PTF (iPTF), with the same goals and facilities but with a slightly different consortium membership. The project uses the CFH12k mosaic camera, with a field of view of 7.26 deg^2 and a plate scale of $1''$ pixel^{-1}, mounted on the Palomar Observatory 48-inch Samuel Oschin Schmidt Telescope (Rahmer et al. 2008). The camera consists of two rows of six $2k \times 4k$ CCDs, one of which is not active.

By the end of Sep. 2014, ∼12,000 deg^2 of sky had been observed by the iPTF in the Mould-R filter[1] and ∼2,300 deg^2 in the SDSS g' filter at least 30 times each. Observations are carried out with several cadences to support various major projects, ranging from searches for comets and asteroids to discovery and monitoring of distant SN. For most of a lunation, the observations are performed in a broad-band R filter. The SDSS g' filter is used during the darkest nights. Under typical seeing conditions ($1.1''$ at the P48 Schmidt) the camera achieves a full width at half-maximum intensity of ∼$2.0''$ and 5σ limiting AB magnitudes of 20.6 in median seeing.

All PTF data taken by the Palomar Observatory 48-inch telescope are automatically routed to two pipelines: a real-time transient detection pipeline optimized for rapid detection of interesting objects, mostly SN, and hosted by the Lawrence Berkeley National Lab, and a longer-term archival pipeline optimized for high-precision photometry and hosted by the Infrared Processing and Analysis Center (IPAC). The IPAC pipeline performs final image reduction, source extraction, and photometric and astrometric calibration (Grillmair et al. 2010; Ofek et al. 2012; Laher et al. 2014). The photometric uncertainty provided by this pipeline is smaller than ∼0.01 mag for $R < 16$ sources and increases to 0.2 mag at $R = 20.6$. The algorithm used for photometric calibration is based on that of Honeycutt (1992) as modified by Ofek et al. (2011) and by Levitan et al. (2011).

The PTF R photometric calibration attempts, within the limits imposed by a survey almost all of whose imaging, especially prior to 2015, was acquired with only a R filter, to reproduce the SDSS r' system. Relative to the reference UCAC-3 astrometric catalog (Zacharias et al. 2010), the astrometric precision of PTF coordinates is about $0.1''$ in RA and Dec.

[1]The PTF Mould-R filter is similar in shape to the SDSS r-band filter, but shifted 27 Å redward.

iPTF, with partial funding from the NSF, is in the process of transitioning to the Zwicky Transient Facility (ZTF), to begin operation in late 2017. The 47 deg^2 field of view of the ZTF camera will be roughly 6 times the area of the PTF camera, and larger than the field of each of the photographic plates used for the Palomar Sky Survey. This, combined with better CCDs with faster readout times, will enable ZTF to observe the sky more than 10 times faster than PTF, while still reaching the same magnitude limit.

3. Sample Selection

RR Lyr stand out in a wide field imaging survey because they are blue and variable. However, the PTF is primarily dedicated to searching for explosive transients. To optimize the cadence for this purpose almost all PTF imaging until 2014 was carried out with the R filter. Thus for stellar broad-band colors we relied on the SDSS (York et al. 2000). In the SDSS the imaging and thus the derived photometry for a variable star was essentially simultaneous for each of the 5 filters.

We developed a probabilistic measure of whether or not a star is a RR Lyr variable based largely on its light curve characteristics. As described briefly in Sesar et al. (2014), we have chosen to use the random forest classifier to isolate a sample of RR Lyr variables from the PTF data. This is a supervised machine-learning algorithm that uses a training sample and a feature set to build a forest of decision trees. Random forest algorithms are able to determine the importance of each feature used for classification and they are not strongly affected by outliers. Random forest classifiers also tend to be less affected by small changes in the training sample than other classification trees because of the random selection of a subset input features at each node, resulting in a selection that maintains accuracy while reducing correlation (Breiman 2001). They are easily applied to very large sets of time series data (i.e. light curves), and have been used extensively on such data sets in the past few years, see, e.g. Richards et al. (2011), Nun et al. (2014), McCauliff et al. (2014), and Carrasco et al. (2014) for QSOs, and in high-energy physics, see, e.g. Sharma et al. (2014). Because of the algorithm's features and its previous success in classifying variable sources, it was selected as the algorithm of choice for the RR Lyrae classifier.

As a supervised algorithm, the random forest classifier requires a training sample and a set of features. After some experimentation, we settled on 10 features to characterize the light curves, including several suggested by Stetson (1996). The training sample consisted of PTF light curves of RR Lyr stars and non-RR objects in SDSS Stripe 82, where the RR Lyr are identified in Sesar et al. (2010), and the remaining stellar objects are non-RR stars. Hernitschek et al. (2016) gives extensive details on a similar selection applied to the

Pan-STARRS PV2 (internal process V2) data. The output of the classifier (denoted Pr, range 0 to 1) is a measure of probability that the light curve under consideration is that of a RR Lyr. The rank ordering of the Pr values is correct, but the conversion to an actual probability has not been quantified. Light curve parameters are also determined, including the period, amplitude, and epoch of maximum light which defines $\phi = 0$.

Experience gained with the random forest classifier suggested that 30 epochs, provided that they are well spaced compared to the typical RR Lyr period, suffice to identify a RR Lyr variable, phase the light curve, and determine its period. We thus require a minimum of 30 detections of a given star for it to be included in the RR Lyr search. Until the fall of 2014, after this sample was originally assembled, the RR Lyrae project had no assigned P48 time. Thus to assemble our sample of candidate RR Lyr stars, we datamined the PTF archive in 2013, searching for high galactic latitude fields that had more than 40 R images. We ran the random forest classifier on the time series of photometry (ignoring images which yielded only upper limits instead of detections) for all stars in such fields that showed evidence of variability and that had 30 or more detections at R. We retained only those with a minimum Pr of 0.70 and which have reddening corrected $g - r$ colors from the SDSS within the range appropriate for RR Lyr, e.g. that of Sesar et al. (2010). As a final check, the NASA/IPAC Extragalactic Database was used to remove known QSOs.

The area on the sky of the Sgr stream within 9° of the orbital plane of this tidal stream (i.e., $|B_{Sgr}| < 9°$, where B_{Sgr} is the latitude in the Sgr stream coordinate system defined in Appendix A of Belokurov et al 2014) was excluded. Other known streams, compiled recently by Grillmair & Carlin (2016), are all closer than 50 kpc and hence not relevant here.

Because the RR Lyr survey with PTF and its successors is largely piggy-backing on the various SN surveys, our sample probes widely separated randomly selected high galactic latitude pencil beam fields, each 7.3 deg^2 in size. Substructure effects should be minimized because of our sparse sampling over a very large area on the sky.

Fig. 1 shows the light curve of one of the brighter RR Lyr in our sample ($r = 56$ kpc) as well as that of one of the more distant RR Lyr ($r = 96$ kpc). The observations extend over more than 6 years with hundreds of detections in the PTF-R filter, and with good phasing throughout. We ignore the Blazhko effect, a modulation with time of the pulsation amplitude seen in some RR Lyr stars, as our light curves in general are not of high enough quality to detect this.

Since the PTF is primarily dedicated to the discovery and study of high amplitude explosive transients such as SN, observations are carried out even when sky conditions (seeing

or transparency) are not optimal, provided it is safe to open the dome. This means that the depth and point source image size for an individual exposure will vary over a wide range as observations of a specific field are accumulated over several years. Many of the PTF images have a limiting magnitude much brighter than that of the median $R = 20.6$ mag (5 σ) limit. Some PTF images, taken under very good conditions (clear night, excellent seeing, excellent telescope performance) reach deeper than the nominal limit. Thus the quality of the light curve of a candidate variable star is not just a function of the brightness of the star and the number of epochs available in the PTF archive. This complicates estimating the completeness corrections in our sample.

We assembled a list of 447 candidate RR Lyr selected from the PTF database to be at a heliocentric distance of 50 kpc or greater at high Galactic latitude[2], with SDSS $(g-r)$ colors from DR10 (Ahn et al. 2014) within an appropriate range and outside the Sgr streams. Fig. 2 shows their location on the sky using Galactic coordinates. Allowing a distance separation of 5%, the closest pair of candidate RRab has a separation on the sky of 0.16 kpc and a distance of 50.5 kpc. There is one other close pair with separation on the sky of less than 0.4 kpc.

Some trends appear within this sample of 447 candidate RR Lyr as shown in Fig. 3, including a trend towards higher median amplitude with approximately constant median period at larger distances. There is also a trend of lower Pr (recall that $0.7 < Pr < 1.0$) towards larger distances; the median probability index decreases from 0.92 for the first bin ($r = 50$ to 53 kpc) shown in Fig. 3 to 0.82 for the last bin ($r > 94$ kpc). These trends are not surprising given that we are approaching the limiting magnitude of the PTF survey at the largest distances probed.

As will be described later, 112 stars were selected selected for spectroscopic observations. These consist of the higher probability RR Lyr candidates from this list, within the constraints imposed by the specific dates of the assigned telescope time.

4. Distances

RRab are almost standard candles, and we adopt a median for their extinction corrected M_R mag (averaging the flux of the best fitting light curve template over one period) of +0.6 mag. However, it is well known that there is a small dependence of luminosity on period

[2]The minimum heliocentric distance of $r = 50$ kpc for a star in our sample corresponds to a Galactocentric distance between 45.9 and 57.8 kpc depending on (l, b).

(linear in log$P$) and on metallicity (linear in [Fe/H]). We first assess the range in period of RR Lyr stars. We use the sample of 173 RRab isolated by Sesar et al. (2010) in Stripe 82 of the SDSS with mean R fainter than 17.0 mag. This sample has excellent photometric data with many observed epochs. It covers a wide range in distance and should be representative of our sample as well. Fig. 4 presents the period-amplitude relation for these stars. The RR type c from the Stripe 82 sample are also shown in this figure. Note that they have have shorter periods and lower amplitudes than do the RRab.

A histogram of the periods for the 173 RR *ab* stars in Stripe 82 with R fainter than 17.0 mag from the sample of Sesar et al. (2010) is shown in shown in the lower panel of Fig. 5; the upper panel displays the same for our PTF RRab sample. The values for mean and rms dispersion of each of the two samples are indicated on the figure; they are essentially identical, which is gratifying, as both probe deep into the outer halo of the Milky Way.

We correct for the period term in the luminosity of RRab adopting the coefficient given by Marconi et al (2015), who present theoretical period-luminosity relations for RR Lyr stars over a range of metallicity based on their new nonlinear time-dependent convective hydrodynamical models of RR Lyr stars. These supersede earlier calculations by Chaboyer (1999), Caceres & Catelan (2008) and others. We note note that their dependence on $\log(P)$ for fundamental mode RR Lyr in the i band is 1.6 times larger than that of Caceres & Catelan (2008) and therefore we may hope that use of their coefficients will provide an upper limit to the change in mean R with both P and [Fe/H].

The luminosity dependence on the period, which is $-1.39\ log(P)$, is in general small, as the median period for our outer halo RR Lyr sample is 0.553 days with $\sigma log(P) = 0.044$ dex. This results in a change in distance of less than 3%; even at the extreme high and low values of $\log(P)$, $P = 0.456$ days and $P = 0.793$ days, the resulting change in distance incurred by including the period dependent term does not exceed 10%. Note that the sample of RRab in SDSS Stripe 82 studied by Sesar et al. (2010) has a median period of 0.582 days, and a σ for $\log(P)$ of 0.044 dex, almost identical to that of our outer halo sample.

Corrections for interstellar absorption were applied based on the reddening map of Schlegel, Finkbeiner & Davis (1998). If a reddening map with larger extinction at high galactic latitude is used, the distances to the RRLyr would increase.

The absolute luminosity of RRab also depends on the metallicity, for which [Fe/H] is used. Schorck et al (2009) have established the metallicity distribution of the outer halo for very low metallicities; the fraction of the stellar content of the Milky Way halo which is extremely metal poor is very small. Again using the coefficients of Marconi et al (2015), we find that potential variations of [Fe/H] of ± 0.5 dex about a (low, but not extremely low)

mean metallicity leads to an uncertainty in the distance of 4%.

Another key issue is the accuracy of the mean R mag measured from our light curves. Although the uncertainty of a R measurement at a single epoch may be large, up to 0.2 mag, the mean R will be much more accurate. A reasonable estimate of this, particularly for stars with many epochs (ignoring upper limits) in their light curves, is 0.03 mag, which corresponds to a distance uncertainty of 1.5%.

Thus if one assumes that the mean metallicity in the outer halo beyond 50 kpc is low and only has a modest gradient with distance and a modest range at any outer halo location, which seems appropriate for the outer halo excluding the Sgr streams, then based on the uncertainties found above, our distances for RRab with good light curves should be precise to 5%. Here the dominant term results from the unknown metallicity. Light curve quality for these RRab will improve with additional observations once ZTF is commissioned resulting in better light curves with more detections.

An empirical test of how large (actually how small) the distance errors might be for RR Lyr due to their range of periods was carried out by B. Sesar. Using the Pan-STARRS RRLyr catalog (to become publicly available on Nov. 1, 2017) he calculated the dispersion in distance based on assuming a fixed absolute R mag, ignoring the period and metallicity dependences, for a large ($\sim$ 200) sample of RRab in the Draco dSph galaxy. He measured a rms scatter of 0.08 mag, corresponding to a distance precision of 4% for this sample. In §3.3 of Sesar et al. (2017b) this test of calculating the dispersion in distance is extended to two additional dSph satellites of the Milky Way, Sextans, and Ursa Minor, again with excellent results. In these tests the metallicity dependence within each of these dSph galaxies was ignored. The metallicity range within Draco extends from [Fe/H] = -3.0 to -1.5 dex (Cohen & Huang 2009; Kirby et al 2011) and the range within Ursa Minor is similar (Cohen & Huang 2010; Kirby et al 2011). Thus the metallicity dependence is not a significant contributor for most, if not all, outer halo stars. It is clear that distances accurate to 5% can be obtained for RRab with high quality light curves.

The above discussion does not address the issue of the the uncertainty in the adopted extinction map. The recent extinction coefficients of Schlafly & Finkbeiner (2011) (their table 6) and the Schlafly et al (2014) dust map lead to somewhat higher extinction at high Galactic latitude than that we adopt, which would result in our distances being slightly underestimated. Furthermore we have adopted an absolute R mag (corrected for reddening) for the median of our sample of +0.6 mag. If this choice is incorrect, all of our distances need to be scaled appropriately.

5. Light Curve Quality

Table 1 gives the light curve parameters for each star in our sample of 112 RRab in the Keck v_r sample. The last three columns of this table indicate for each RRab the number of available R-band detections, the number of g-band detections, and an assessment of the light curve quality in the PTF Stellar Light Curve database as of late 2016. The latter was set by visual inspection by the first author in late 2016. Quality 1 light curves are clearly RR Lyr variables, quality 2 are probably RR Lyr, while the nature of objects with quality 3 light curves is uncertain.

The initial determination of light curve parameters for the Keck v_r sample was carried out in 2014, at which time the number of available epochs was smaller (often considerably smaller) than at present. Beginning in late 2014 we were allocated a total of roughly 100 hours of P48 (i.e. PTF) time made available through the Caltech allocation to improve the light curves of the more distant stars in the Keck v_r sample. These distant stars have a much higher fraction of non-detections than do the brighter end of our sample, and so need additional imaging to raise the number of detections to a level that ensures accurate characterization of the light curve parameters. Our goal in this effort is 100 detected epochs of R-band imaging for each of the most distant RR Lyr candidates.

In late 2016 and early 2017 the light curve of each of the stars in the Keck v_r sample was checked to look for problems in the phasing, i.e. incorrect periods or determinations of $\phi = 0$ caused by the limited data available when the light curves were first determined in 2014. As necessary, the light curve parameters were re-determined at that time, and the correction from the observed v_r to the systemic v_r described in §6 was updated using the new ephemeris parameters. This was a crucial step, as the initial values were in several cases sufficiently far off that the accumulated phase change over several years significantly affected the derived phase correction to the observed v_r.

At the present time, as indicated in Table 1, only 12 stars from the Keck v_r sample of 112 stars have less than 50 detections in R or 50 detections in the g filter. Only 4 stars (4%) of the total sample of 112 RR Lyr are classified as having poor light curves (i.e. quality 3). As described earlier, we have until very recently had no control over the observing plan for PTF/P48 time, which is defined by the other major projects of the PTF, especially the SN projects. Thus the number of epochs of observation of a given star varies from a minimum of $\sim$30 up to $\sim$700 when a RR Lyr candidate is by chance located in a field which is of major interest to one of the other PTF projects.

6. Radial Velocity Measurements

A spectroscopic campaign to obtain radial velocities for RR Lyr candidates began at the Keck Observatory with the Deimos spectrograph (Faber et al. 2003) in the spring of 2014 following a brief effort to use the DBSP on the Hale Telescope at the Palomar Observatory, which yielded one useful spectrum. RRab are pulsating periodic variable stars. Spectroscopic observations to determine v_r must be taken within the range of phase such that (dv_r/dt) in the stellar atmosphere is as small as possible. The observing list for each night was compiled from the candidate RRab near the meridian during the night with the appropriate range of phase ($\phi = 0.1$ to 0.7) accessible during that time. Observation planning therefore required having both a coordinate list and accurate predicted phases from the start to the end of the night for the specific date; the phases are calculated from the periods we determined from the PTF light curves. Candidates with high probability index ($Pr > 0.9$) were favored, but it was sometimes necessary to incorporate candidates with lower Pr to fill in gaps in the observing plan for a specific night.

The Deimos spectrograph was usually configured with the 600 grove/mm grating blazed at 7500 Å and spectral resolution ∼2000 for a 1.0 arcsec wide slit and a scale of 0.65 Å/pixel. Spectra were taken with the central wavelength set to 7500 Å. Most spectra were taken with a 1.0 arcsec wide slit, but on nights with good seeing, the 0.7 or the 0.8 arcsec slit was used, yielding correspondingly higher spectral resolution. During our first Keck run, a small number of spectra were acquired with the 1200 g/mm gold coated grating blazed at 7545 Å which yielded even higher spectral resolution. However, the velocity precision for an exposure of a fixed time turned out not to be better than with the 600 g/mm grating due to the increased SNR with the 600 g/mm grating. The maximum (and typical) exposure time was set to 30 min to avoid excessive phase blurring. Fig 6 shows spectra in the region of Hα for 9 of our RR Lyr candidates selected to cover the full range in distance of our sample. Note the degradation in the SNR at the largest distances, which arises from the fixed maximum integration time of 30 min.

The determination of the systemic v_r for a RR Lyr requires knowledge of the phase at the time of the observation. A correction which depends on the phase is applied to get the systemic v_r, then a heliocentric correction, and finally we apply a correction to the Galactocentric rest frame (GSR).

The uncertainties in the systemic velocities include both a measurement error and a term for the uncertainty in fitting to the model radial velocity curve. Details for this calculation are given in §5.3 of Sesar et al. (2012). Since typical v_r amplitudes over the period for RR Lyr stars of Hα are ∼110 km s^{-1}, it is important that the phase of observation be determined accurately. This requires accurate periods and phasing.

The primary feature we use for v_r determination is Hα. Due to the low efficiency of Deimos in the blue, we do not achieve a SNR high enough there to use the higher Balmer lines or the strong blue metallic lines. Sesar (2012) has derived template velocity curves which calibrate the change in velocity as a function of pulsation phase for several of the Balmer lines; we adopt his Hα template here; see also the very detailed recent study by Chadid, Sneden & Preston (2016). The normalized $v_r - \phi$ curves of Sesar (2012) are then scaled by the amplitude of variation of the light curve to derive the correction from the observed v_r at phase ϕ to the systemic velocity. The other major features clearly visible in these spectra are the Paschen lines around 8600 Å, but we are not aware of any $v_r - \phi$ calibration for them. The infrared Ca triplet and a few OI lines are also visible in these spectra, and we will undertake an attempt to use them as metallicity indicators in the future.

Standard arc lamps (Ne, Ar, Kr, and Xe) were used for wavelength calibration, which was then tuned up slightly for each observation of a RR Lyr candidate using the night sky emission lines superposed on each stellar spectrum, important as there are few arc lines in the region of Hα, the primary feature we are using to determine v_r.

From our Keck runs beginning in April 2014 and extending through Sep 2016 we have acquired spectra of roughly 135 candidate RR Lyr from our PTF sample, 112 of which we believe to be RRab stars based on their light curves, their colors, and their spectra, the remainder being a few quasars, a few RR type c variables, or other types of variable stars. The stars in the Keck v_r sample are widely dispersed on the sky with the closest pair in the list of candidate RRab being separated by 0°.2. Thus no multiplexing was possible, and a substantial number of Keck nights were required to obtain this set of spectra.

The set of 112 RR Lyr with spectroscopic v_r, which are listed in Table 1, have heliocentric distances of $50 < r < 109$ kpc with a median of $r = 73$ kpc. The resulting v_r relative to the Galactic standard of rest and its uncertainty are given in Table 2. Typical uncertainties for v_r from a single measurement range from 17 to 20 km s^{-1}.

A separate list of 4 RR Lyr that were observed during our first run with Deimos on Keck for this project, but which are probably part of the Sgr stream, is given at the end of this table. The exclusion region for the Sgr stream was originally set to be within 5° of the orbital plane of this tidal stream, but was raised to 9° shortly after observing commenced. Once the exclusion region around the Sgr stream was increased in size, these four stars were dropped from our sample of candidate RR Lyr in the outer halo of the Galaxy. There are 7 stars in our sample which are between 9 and 15° from the orbital plane of the Sgr tidal stream.

6.1. Test of v_r Accuracy

To demonstrate the accuracy of our systemic v_r for RR Lyr variables, Table 3 gives the independent v_r for those candidate RR Lyr variables from our sample with more than one Deimos spectrum; there are 22 ($\sim$20% of the total sample with Keck v_r) with two independent spectra. In several cases, the two Deimos spectra were taken on the same night, often consecutively, but analyzed independently. The agreement between the two determinations of $v_r(GSR)$ for each of these 6 stars is good. There are 11 stars with two spectra from the same night or from consecutive nights. These in general show small differences in v_r between the two spectra. Only three have differences exceeding 20 km s^{-1}, with the largest difference being 33 km s^{-1}. Given that the nominal uncertainty of a single measurement is $\sim$20 km s^{-1}, this agreement is good.

There are 8 RR Lyr candidates with two Deimos spectra taken more than a year apart. The differences are larger here, ranging from 9 to 51 km s^{-1}, with two having differences exceeding 40 km s^{-1}.

The difference in v_r for stars with multiple spectra is shown in Fig. 7 as a function of the separation in time between the two epochs of observation, which increases along the X axis. As indicated above, for small differences in time, the difference between the two v_r for a given star is within close to or within the expected uncertainties, but once the time interval becomes large (months to years), there are two cases with disagreements exceeding 40 km s^{-1} between the two derived v_r.

We suspect that these disagreements arise in part from possible errors in the phases due to uncertainties in the period. Thus our process to determine v_r in the Galactic standard of rest (GSR) for these RR Lyr variables from the observed v_r using phase dependent corrections appears to be working reasonably well in general. However, for a small fraction of our candidate RR Lyr variables, this is not the case. While there are a few unexpectedly large discrepancies, they are relatively small compared to the velocity dispersion among our 112 RRLyr sample to be discussed later in §7.

As indicated earlier, if the star were not a genuine RRab variable or the key light curve parameters (period and epoch of zero phase) we derived were wrong, incorrect v_r would be derived. However, we note that one of the stars with two independent spectra which shows an unexpectedly large $\delta(v_r)$ has an excellent light curve with 224 detections with the PTF-R filter.

6.2. Contaminants in the Sample of Candidate RR Lyr Stars

The only blue point sources seen at high galactic latitude are RR Lyr, QSOs, blue horizontal branch (BHB) stars and blue stragglers. Since our primary selection is by variability resembling that expected for a RRab, the non-variable BHB stars and blue stragglers become irrelevant. Thus the primary source of contamination is expected to be QSOs, but the timescale and characteristics of their variation are quite different from those of RRab. As the number of observed epochs of photometric monitoring increases, and this will grow with time as the iPTF transitions into the ZTF, the fraction of contaminating quasars will fall, because their extended light curves will diverge more and more from those of RRab, the variation will not be periodic, etc.

Table 4 lists the five broad lined objects (i.e. QSOs) we have found from our spectroscopic campaign that are not included in NED. Given that most QSOs are eliminated as they do not have light curves that resemble RR Lyr and adding in a check with NED, the contamination rate of QSOs within the sample selected for spectroscopy can be kept very low, and can, as described above, be expected to fall with time as the survey time coverage increases. WISE colors (Wright et al. 2010) can also be used to cut down the fraction of QSO contamination (Nikutta et al. 2014) due to the difference in spectral slope between a power law and a (hot) thermal spectrum, but are of limited use for such distant objects as they are often so faint that only the W1 color is given in the WISE catalog.

The other potential contaminant of our sample of RRab stars is overtone pulsators, i.e. type *c* RR Lyr. Several of the variable stars listed at the end of Table 4 are probably RR Lyr *c*. They were originally believed to be RRab and were part of the spectroscopic sample, but as their light curves built up with time, they became inconsistent with the period range and/or shape appropriate for RRab and were removed. Given the mean difference in luminosity at R of $\sim$0.25 mag between RR Lyr pulsators in the fundamental and the first overtone modes, the distance of a candidate will be overestimated by 12% if it is actually a type *c* rather than the more common type *AB* RR Lyr. Furthermore the $v_r - \phi$ relationship for Hα of the overtone pulsators may be different from that derived for the RR Lyr *ab* that we are using.

Most importantly, type *c* RR Lyr can be eliminated using a period-amplitude diagram, as is shown for the SDSS Stripe 82 sample in Fig. 4. The type *c* variables have smaller periods and smaller amplitudes of variation than do the fundamental mode RR Lyr *ab*. There is essentially no overlap between them in this diagram.

7. The Radial Dependence of The Velocity Dispersion

Our ultimate goal is the determination of the mass of the MW out to as close to the virial radius as possible. We intend to use our sample of RR Lyr as massless point-source test particles. In support of this effort, we have ignored RR Lyr in the Sgr stream. However, there may be previously unknown structures whose stars may be moving with non-virialized velocities. So before determining the velocity dispersion, we look for evidence from our data regarding the possible presence of new substructures. A search for previously unknown low luminosity galactic satellites in the outer halo that have not yet been disrupted was conducted by Sesar et al. (2014) by using the RR Lyr from the PTF as indicators, but there was no detection, although the derived upper limit is high. With our v_r survey we can look for evidence for the presence of more diffuse and more extended structures.

At the large distances we probe, the dispersion of the line-of-sight velocity, which is what we measure, is essentially identical to the dispersion of v_r, the radial velocity as seen from the Galactic center. We first consider the sample as a whole. Fig. 9 shows a histogram of the entire sample of 112 RRab. We see a rather broad range spread between -220 and $+220$ km s^{-1}. This may be the result of a wide spread in v_r at all Galactocentric distances, of a trend with r, of the presence of outliers due to halo structures, or of contamination in the sample with objects that are not RRab. As discussed in 6.2, we believe that our sample has few such contaminants.

In an effort to identify whether outliers are present, we carried out an exercise where we began with the full sample, calculating the v_r, $\sigma(v_r)$, and the median distance. We then removed the largest outlier in $|v_r - < v_r > (last)|$, where "last" refers to the mean v_r found in the previous iteration. We continued doing this repeatedly. The result for v_r, $\sigma(v_r)$, and the median distance for is shown in Fig. 10 for 24 such trials. First we note that the median distance begins for the entire sample at 74.1 kpc and slowly decreases, ending up after 24 deletions at 71.8 kpc. The $\sigma(v_r)$ for the entire sample treated as a whole begins at 98 km s^{-1} and ends up at 60 km s^{-1}. It falls quite rapidly initially, suggesting the presence of some outliers, then after about 8 RRab are removed, the decline becomes more gradual. At the same time, the mean v_r starts at about -19 km s^{-1}, and rises to $+3$ km s^{-1} at the end of the 24 trials. So the halo has no, or at most very small, net motion.

To proceed further, we need to look into potential variations with distance and to whether we can find any more clues regarding the presence of outliers. The $v_r(GSR)$ we have determined for 112 candidate RR Lyr with distances beyond 50 kpc in the MW halo are shown as a function of r in Fig. 11. In this figure, the stars are divided into three distance regimes, with the intermediate one being 70 to 85 kpc, and the most distant group, which contains 26 stars, ranges outward from 85 kpc to 109 kpc, with four at distances exceeding

100 kpc. The first point to note is that the mean $v_r(GSR)$ for each of the three groups (shown as large stars in the figure) is close to 0 km/s; the mean values and other statistics are given in Table 5. This is yet another indication that our values of $v_r(GSR)$ inferred from our v_r, as corrected for phase within the RR Lyr period, are in general valid.

Before computing the velocity dispersion, we need to decide whether there are genuine outliers and how to handle them. These are important as they may be a manifestation of previously unknown large scale substructures in the halo. Fig. 11 shows several outliers, and we have chosen $|v_r| < 200$ km s^{-1} as the cutoff for outliers for the sample within 85 kpc, dropping to 170 km s^{-1} outside that distance. The number of outliers in each distance range is given in Table 5. With this definition, there are a total of 9 outliers from the 112 RRab in our Keck v_r sample. They are circled in Fig. 11.

We first look at the low outliers. There are only five major low outliers. These five RR Lyr have $v_r < -200$ km s^{-1}, and distances between 51 and 73 kpc. All of them have excellent quality 1 light curves. Fig. 8 shows the position on the sky of the 112 RR Lyr candidates in our Keck/Deimos v_r sample. These 5 low outliers (indicated as blue stars in the figure) are confined to a small region on the sky with RA between 329 and 10° and Dec between 4 and 15°. A blowup of this region on the sky is shown in Fig. 12. The green points indicate RR Lyr in the Pisces overdensity, discovered by Sesar et al. (2007) as a linear stream at a distance of ∼80 kpc within the SDSS stripe 82; however recall that Stripe 82 is a narrow equatorial stripe only 1°.27 wide extending from R.A. 20^h to R.A. 4^h. A more recent discussion of this structure is given by Nie et al. (2015), but this structure is more distant than the set of 5 low outliers in our sample. An examination of Figs. 8 and 12 combined with Fig. 11 strongly suggests that these five stars belong to some previously unknown diffuse outer halo structure which extends over about 40°, perhaps from a disrupted satellite. These five low outliers are sufficiently far from the plane of the Sgr streams that it is unlikely that they are part of it. We therefore consider them as potentially not virialized. The choice of the v_r cutoff adopted for RR Lyr with $r > 85$ kpc of $|v_r| < 170$ km s^{-1} is an estimate based on Figure 11.

Table 5 gives the statistics of the sample of 112 RR Lyr when divided into three distance ranges, and when only two groups are used, with a boundary at 85 kpc. Values for $\sigma[v_r(GSR)]$ are given as calculated from the measured $v_r(GSR)$ of each RR Lyr, and also with a 20 km s^{-1} measurement error removed. They are calculated for the full sample, and also for the case where the major outliers have been excluded. Since the removal of only a few outliers considerably reduces the velocity dispersion within each distance range, we consider our choice of cutoffs for outliers as reasonable. For example, for the outermost group of RR Lyr with $r > 85$ kpc, $\sigma[v_r(GSR)]$ is reduced from 90 km s^{-1} to 65 km s^{-1} by

removing only 3 outliers from our sample of 26 RR Lyr in this distance range.

Note that with the outliers eliminated, the velocity disperion is quite low, not exceeding 87 km s^{-1} beyond 50 kpc, and for the outermost stars with $r > 85$ kpc, $\sigma[v_r(GSR)] \sim 65$ km s^{-1}. Clearly a larger sample of tracers with accurate distances and v_r beyond 50 kpc is desirable. We are working on it, but it will take several years to enlarge our sample of 112 RRab beyond 50 kpc with measured v_r by a substantial factor.

8. The Radial Distribution of the PTF RR Lyr Sample

With considerable caveats, we present the radial distribution in the outer halo of the MW for our sample of 447 RR Lyr candidates. We assume an isotropic spherical halo. The major concern is the serious incompleteness in our sample of outer halo RR Lyr stars at the largest distances probed, i.e. beyond 90 kpc.

One might also worry about an increasing number of interlopers (i.e. not genuine RRab) in the sample as the distance increases and the light curve quality decreases due to increasing observational uncertainties in each individual observation and to a lower fraction of detections coupled with an increasing fraction of upper limits for a given number of epochs of observation. However, the small spread of the period distribution and the strong period-amplitude correlation shown in Figs. 5 and 4 as well as the behavior of the quartiles of period and amplitude as a function of distance (see Fig. 3 suggest that our sample is not contaminated by interlopers even at the largest distances we probe. Note that a careful examination of Fig. 3 does support the suggestion that there is a strong increase in incompleteness of our sample of RRLyr at the largest distances included our sample.

We can assess the importance of incompleteness by considering the fraction of upper limits instead of detections among RRab which have many epochs of observation and which span the full range in distance probed here. Fig. 14 shows some relevant data, specifically the fraction of upper limits among the available images in the PFS database for a sample 80 RR Lyr stars at the close end of our sample (∼50 kpc) vs 50 of the most distant ones (i.e. beyond 95 kpc). As we had no control over the cadence nor of the selection of fields to be observed on a given night at that time, the number of observations of a given field (at least at the time that the sample was constructed) depended on how many times a field was observed by other PTF projects.

For the nearer RR Lyr in our sample, the fraction of upper limits is low, usually less than 10%, while for the most distant ones, the fraction of upper limits is typically ∼60%. Our PTF RR Lyr sample was selected in 2014 and hence given the much smaller number

of images of each field in the database at that time compared to the present values given in Table 2, a larger fraction of the most distant RR Lyr will not be picked up as candidate RR Lyr as their light curves would not have contained more than 30 detections at that time. Although as indicated earlier in §5, the ephemerides have been checked recently and updated as necessary, the list of candidates has not. Redoing the selection from the PTF seems unjustified given that a high quality PS1 RR Lyr catalog with careful determination of its completeness and purity will be released shortly (Hernitschek et al. 2016; Sesar et al. 2017b). We can safely assume that there is an incompleteness of at least a factor of two for the most distant part of our sample; the actual completeness correction at the faint end of our PTF sample could be even larger.

With regard to the issue of contamination of the Keck v_r sample by interlopers, we compare the number of candidate RR Lyr with $Pr > 0.8$ as a function of distance with the distribution in distance of our sample of 112 RR Lyr with Keck/Deimos v_r. Note that 326 of the 447 candidates meet this probability restriction, while essentially all of candidates selected for Keck spectroscopy have $Pr > 0.8$. This ratio is given as a function of distance in Table 6. There are many candidates at the near end of the sample, but our goal was to get spectra of as many distant stars as possible, so candidates at the closer end of our sample were not observed unless no suitable distant candidate had a phase within the allowed range during that part of the night. As shown in Table 6, only 21% of the candidates with $r < 64$ kpc have Keck v_r, while this fraction is ∼50% from 64 to 99 kpc, beyond which it drops to ∼38%. If the sample of candidates was seriously contaminated with interlopers as the distance increased, this success fraction should have fallen significantly. We can therefore assume that the fraction of interlopers is not rising significantly towards the faint end of the sample, until a distance of at least 90 kpc, beyond which the sample is small.

Another way to approach the same issue is to examine the current PTF light curves for those RR Lyr candidates which are not in the Keck v_r sample. If there is serious contamination which is dependent on distance by stars which are not RRab (presumably more contamination at larger distances), the fraction of these RR Lyr candidates that have quality 3 light curves (light curves which do not suggest that the star is a RR Lyr) will rise substantially with distance. We have carried out this check for candidates over a wide range in distance. For candidates at distances closer than 60 kpc, 94% of them show high quality light curves. This fraction falls to 85% for those between 65 and 70 kpc. It remains above 80% out to 95 kpc, beyond which it drops to ∼70%. This change with distance of the potential fraction of contaminants is small enough that the effect on the power law fit should not be large, at least within 95 kpc.

Fig. 15 presents the number of candidates in bins in distance, with both axes of the plot

using a logarithmic scale. Also shown are a number of power law fits. The upward arrow indicates a correction for an incompleteness of 50% in the RR Lyr sample at the largest distances probed arising from the large fraction of upper limits in their PTF light curves. It is clear that a volume density law of $\rho(r) \propto r^{-4}$ is a reasonable fit from 50 to 85 kpc, and, with an incompleteness correction of a factor of two, would be a good fit out to 100 kpc.

9. Comparison With Previous Results

9.1. Comparison With Other Samples of Milky Way Outer Halo Stars

As a result of many recent large stellar surveys, our knowledge of the outer halo of the MW is improving very rapidly. Outer halo stellar samples are increasing in size and distance range probed. For comparison, the early discussion of the kinematics of the halo by Kinman et al. (1996) used only a total of 67 RR Lyr and BHB stars in the inner halo out to $r < 15$ kpc; they found a velocity dispersion of $\sim$110 km s^{-1}. However, samples of outer halo stars with spectroscopic v_r, particularly in the crucial region beyond $r = 80$ kpc, such as ours are growing very slowly.

The Catalina Real-time Transient Survey (CRTS) has been in operation since 2006 mining the data stream from three telescopes (0.7 m, 1.0 m, and 1.5 m diameters) in the mountains north of Tucson Arizona which are operated by the Lunar and Planetary Laboratory at the University of Arizona and whose primary mission is the detection of near earth asteroids. The photometric calibration and cadence of the CRTS are not as well controlled as those of the PTF, but the time span of the imaging and hence of the light curves is more than a decade. Drake et al (2014) used this database to produce the Catalina Surveys Periodic Variable Star Catalog, which has roughly 16,800 RRab variables. The maximum distance of the RRab in their survey is $\sim$60 kpc, however the bulk of their sample is closer than 40 kpc. Our sample begins at 50 kpc and we have eliminated the Sgr stream, while the CRTS catalog has not. We find that the overlap between our sample of 447 RR Lyr and their sample is only 32 stars. The agreement of the derived period for the variables in common between the two surveys is less than 0.0010 days for 24 of the 32 stars in common, while the largest difference is 0.0016 days. The more recent southern extension of the Catalina Sky Surveys RR Lyr catalog, Torrealba et al (2015), has no overlap in sky coverage with our Palomar based survey.

Very recently Iorio et al (2017), in a paper not yet accepted, have produced a catalog of RR Lyr by combining the first GAIA data release (GAIA collaboration 2016) with 2MASS (Skrutskie et al 2006). Their sample has $\sim$21,600 RR Lyr and is confined to the inner halo.

Thus there is a very large overlap with the CRTS sample of Drake et al (2014), but Iorio et al (2017) only reach out to a heliocentric distance of 20 kpc, and thus there is no overlap with our sample, whose minimum distance is 50 kpc.

The huge database of SDSS, coupling uniformly measured multi-color photometry from its deep imaging over a large fraction of the northern sky and uniformly reduced spectra, was a breakthrough. It was used by Xue et al. (2008) to isolate a sample of ∼2400 BHB stars with v_r that reaches out to $r \sim 40$ kpc, with very limited coverage out to 50 kpc; Xue, Rix, Yanny et al. (2011) gives a slightly improved selection of BHB stars from the same material. More recently, Xue et al. (2014) used the database of the Sloan Extension for Galactic Understanding and Exploration (SEGUE) (Yanny, Rockosi, Newberg et al. 2009) to select a sample of 6036 distant K giants. They developed probabilistic procedures to obtain their luminosities, claiming to thus have achieved a median accuracy of 16% in their distances. Their sample extends out to ∼80 kpc, although almost all of the stars beyond 60 kpc are in the Sgr Stream or other known halo substructures.

The K-giant sample of Xue et al. (2014), when cleaned of known substructures, primarily the Sgr Stream, has 1757 stars with distances beyond 10 kpc, but in the outer halo it is significantly smaller than our sample, which begins at 50 kpc. The purged sample of Xue et al. (2014) has only two K giants beyond 65 kpc, with the most distant at about 75 kpc. Our sample reaches significantly further out in the MW halo with a median distance of 73 kpc. Furthermore, the distances to our RR Lyr sample are much more accurate than those of K giants.

The hypervelocity star survey (Brown, Geller & Kenyon 2014) has carried out extensive spectroscopy of very blue stars in the outer halo selected from SDSS photometry. While SDSS colors are used, this is one of the few surveys besides ours that obtains their own spectra. The kinematics of the majority of their sample of the late B-type outer halo stars found the course of this work are discussed in Brown et al. (2010). Their dataset contains 910 late B and early A such stars, almost all of which are BHB stars with a small contamination of less luminous blue stragglers. The bulk of their sample is closer than 50 kpc.

Bochanski et al. (2014) selected a sample of 404 candidate very distant M giants based on their NIR colors from UKIDSS combined with optical colors from SDSS and undetectable proper motions (to rule out nearby M dwarfs). Two of these were spectroscopically confirmed and appear to be extremely distant, with their estimated minimum distances being 130 kpc. Their sample of very distant M giants selected via photometry has roughly 80% contamination which can only be resolved by spectroscopy; photometry alone is insufficient. Furthermore, M giants in the outer halo are a very biased indicator as they can only arise from a metal-rich population, and presumably are located in potentially non-virialized ini-

tially compact infalling structures, if in fact their distances and classifications are correct. As noted by Bochanski et al. (2014), these stars lie close to the Sgr plane. The recent model of the Sgr Stream by Dierickx & Loeb (2017) suggests these M giants are located within the Sgr Stream; it successfully reproduces their distance and low $v(GSR)$. Sesar et al (2017c) have recently identified some of these spurs in the Sgr stream at distances exceeding 100 kpc using the PS1 RR Lyr sample. However, given the high contamination fraction of their M giant sample, the amount of observing time which would be required to generate a clean large sample of such distant M giants is prohibitive and furthermore a sample of M giants would not probe the bulk of the outer halo of the MW.

Slater et al. (2017) isolate a sample of ∼4000 distant giants in the halo with wide field imaging using a narrow bandwidth filter covering the region of the Mg triplet at 5170 Å, which is well known to be a good giant/dwarf discriminator. This is combined with broad-band SDSS imaging. Extensive statistical treatment using population synthesis modeling is required to clean the sample of numerous dwarf interlopers, and the distances of individual objects are quite uncertain. The sample of ∼4000 giants reaches out to 80 kpc.

Deason et al. (2012) attempted to build up a sample of more distant ($D > 80$ kpc) BHB stars by stacking multi-epoch photometry from Stripe 82 of the SDSS (and other regions with multiple images) to isolate candidate BHB stars, but these are too faint to have SDSS spectroscopy. They obtained low resolution ($\lambda/\Delta\lambda \sim 800$) spectra using FORS2 on the VLT to try to separate BHB stars from contamination by brighter blue stragglers, which outnumber by a factor of more than four the desired BHB stars. The final sample has only 7 faint BHB stars. Deason et al. (2012) then add a small number of other potential outer halo stars with highly uncertain distances as well as the dwarf satellites of the MW.

The only sample that reaches out to the distances probed by our RR Lyr sample with a substantial number of stars beyond 50 kpc is that of Deason et al. (2014) which uses BHB and blue straggler stars from the SDSS DR9. There are several issues that afflict this sample, particularly contamination with blue stragglers, and, more seriously, with QSOs. Extensive color modeling, taking into account photometric scattering, was used to try to remove contaminants, which outnumber the desired BHB stars by a large factor.

It is clear that the sample of distant RR Lyr from the PTF with Keck radial velocities presented here has unique characteristics. It is a clean sample with few interlopers, and each star has has a highly accurate distance. At the present time, and even after the release in Nov. 2017 of the PS1 sample by Sesar et al. (2017b), ours is the only reliable sample with at least a modest number of of tracer stars beyond 80 kpc in the outer halo with measured v_r.

9.2. The Density Profile in the Outer Halo

The determination of the density profile in the outer halo of a large set of massless tracer stars is clearly a crucial input to determining the mass of the MW. Given the limited data, the solution is usually expressed as a power-law fit to the density vs distance. Our preliminary result based on a large sample of RR Lyr variables is given in §8 and is shown in Fig. 15. We find that a power law in r with a slope of ~ -4 is consistent with the stellar density $\rho(r)$ derived from the distances of our RR Lyr sample. This assumes an isotropic spherical halo. With larger samples one can also solve for the flattening profile of the halo, but we could not attempt this. Bovy et al. (2017), based on an analysis of the Pal 5 and GD-1 stellar streams, suggest that the axis ratio of the dark matter's halo density distribution is 1.05 within the inner 20 kpc, providing some support to our assumptions, although Iorio et al (2017) suggest that the inner halo has a substantial oblateness which decreases at larger Galactic radii. There seems to be a general consensus that the outer halo is less oblate than the inner halo.

Our result contradicts that of Deason et al. (2014), who claim that beyond 50 kpc there is a striking drop in the stellar halo density. Although in their earlier paper (Deason, Belokurov & Evans 2011) they found a power law fit of $\alpha = -4.6$ for the region $27 < r < 40$ kpc (the maximum r reached), Deason et al. (2014) find a power law slope of -6 beyond 50 kpc, with even steeper slopes (power law index -6 to -10) favored at larger radii. On the other hand, De Propris et al. (2010), who used a sample of 666 BHB stars from the 2dF quasar redshift survey, found a very shallow slope for the density in the outer halo of -2.5 ± 0.2 and a velocity dispersion which increases with r, reaching a huge $\sigma(v_r)$ exceeding 200 km s^{-1} at $r \sim 80$ kpc over the two lines of sight probed. Our data do not support the results of either of these two studies. Our sample is much cleaner with much better distances than the samples of either of these two analyses.

A number of other analyses have been published recently which agree with our halo density distribution to within the uncertainties. Among the many samples of outer halo stars discussed above in §9.1, the large SDSS/SEGUE samples of K giants stand out for their size and spatial coverage. The latest analysis of such is that of Xue et al. (2016). As the luminosity of K giants depends strongly on the metallicity, they had to use forward modeling techniques to fit the spatial distribution and abundance distribution simultaneously. They found that a power-law slope with index -3.8 ± 0.1 is a good fit to the number density profile of the halo beyond $r \sim 20$ kpc. Das & Binney (2016) reanalyze this sample using an extended distribution function to find the density distribution power law index is -4 at large radii out to 80 kpc. Kafle, Sharma, Lewis et al. (2914) combine the BHB and K giant samples from the SDSS/SEGUE to find a slope of -4.5 in the halo beyond $\sim$20 kpc.

The recent work by Slater et al. (2017) using SDSS photometry coupled with imaging in a narrow band filter centered at the Mg triplet to eliminate dwarfs also targets K giants. They use sophisticated CMD modeling and population synthesis to derive a halo density profile $\rho \propto r^{-3.5}$ from 30 to 80 kpc.

Thus, as discussed above, there seems to be a growing consensus that in the outer halo of the MW at least out to 85 kpc, the stellar density can be represented as a power law with a slope of -3.5 to -4. This is quite close to the slope found in the inner halo, at least from 20 kpc outward, by several groups, see e.g. Xue et al. (2016).

9.3. The Velocity Dispersion In the Outer Halo

The behavior of the v_r of a sample of massless tracers as a function of distance provides important clues as to the potential and total mass of the MW. Towards this goal, several of the studies referenced in §9.1 have measured v_r for a large fraction of the members of their sample. In particular those based on SDSS and its successors (i.e SEGUE) fall into this class. In this section we compare our derived $\sigma(v_r)$ as a function of distance for our RRab sample (shown in Table 5 and in Fig. 13) with those of other groups.

The two large samples of outer halo stars based on the SDSS and SEGUE, i.e. the BHB sample of Xue et al. (2008) (see also Xue, Rix, Yanny et al. 2011) and the K giant sample of Xue et al. (2016), both of which reach out to $r \sim 50$ kpc, have been analyzed by many different groups using various sophisticated modeling techniques to derive properties of the outer halo. The latest result from these samples is Xue et al. (2016), where references to earlier work can be found.

Xue et al. (2008) and Xue, Rix, Yanny et al. (2011) derived the radial trend of $\sigma(v_r)$ out to 50 kpc, where they found $\sigma(v_r)$ $\sim$95 km s^{-1}. The spatial range of this relation was extended by Deason et al. (2012), who added a small number of more distant objects. Kafle, Sharma, Lewis et al. (2914), who derived their own sample of K giants from the SEGUE data, also found a similar value of $\sigma(v_r)$ of $\sim$100 km s^{-1} for $r \sim 50$ kpc; see their Fig. 1.

Fig. 13 illustrates some of these results from the literature compared to our relationship for $\sigma(v_r)$ as a function of r between 50 and 100 kpc. With the exception of De Propris et al. (2010), all of these investigations, including ours presented here, are in reasonable agreement regarding the velocity dispersion of the outer halo stars as a function of distance from 50 to 100 kpc within the regime probed by each group, 50 to 100 kpc in our case. All recent studies find $\sigma(v_r)$ $\sim$90 km s^{-1} at 50 kpc, dropping lower as r increases. The hypervelocity

star survey (Brown, Geller & Kenyon 2014) derives the same general decline of $\sigma(v_r)$ with r but has $\sigma(v_r)$ roughly 20 km/sec higher at all r probed than our result and that of most recent work.

The agreement on the spatial distribution $n(r)$ among the various studies, among the most recent of which is Xue et al. (2016), is also satisfactory out to perhaps 60 kpc; from ∼30 to ∼60 kpc all groups agree that the number density of tracers can be represented by a power law with index of about −4. There are only two surveys beyond that, our work and that of Deason et al. (2014), and there is a major disagreement at these larger distances between us, with Deason et al. (2012) claiming a very rapid drop in the number density beyond 50 kpc. They find a power law of −6 with distance beyond 50 kpc, dropping to slopes of −6 to −10 at larger distances. Unless we have badly underestimated our contamination problems, which at least in the sample selected for Keck spectroscopy is highly unlikely given the quality ratings of the light curves and the period-phase relation for our sample shown in Fig. 4, we advocate that our results are more reliable, given the substantial contamination of the Deason et al. (2012) sample by QSOs for which the corrections they use may not be adequate.

We thus conclude that the outer halo at $r > 70$ kpc is cold, and it's radial velocity dispersion is low. These factors suggest, in accordance with several recent analyses, a low total mass for the MW. For our RRab survey based on the PTF database, the key issues are the purity and completeness of the sample and the potential impact of substructure which we suggest may produce the outliers in v_r in these distant outer halo samples of "massless and virialized" tracer stars. The new PanSTARRS RR Lyr catalog by Hernitschek et al. (2016) and by Sesar et al. (2017b) will allow future investigations to avoid most if not all of these concerns.

10. Summary

RR Lyr stars of type ab are ideal massless tracers that can be used to study the outer halo of the MW. Because they have (to first order) a fixed luminosity, their periods are about 0.5 days, they are common in old metal-poor stellar populations, and their amplitude of variation is substantial, reaching up to ∼1 mag, they are easily found in any multi-color imaging survey with extensive temporal coverage. Since they are blue, even when they are in the outer halo of the MW, they stand out against the numerous redder foreground stars, and can be distinguished from quasars by the nature of their variability, quasars being non-periodic variables, while the other blue halo stars (BHBs and blue stragglers) can be eliminated as being non-variable. RR Lyr are thus ideal probes of the outer halo which

can be found at great distances in the current generation of large stellar surveys and whose distances can be measured to high accuracy with just a light curve.

We present here a sample of 112 RRab beyond 50 kpc in the outer halo of the MW for which we have obtained moderate resolution spectra with Deimos on the Keck 2 Telescope. Four of these have distances exceeding 100 kpc. These were selected from a much larger set of 447 candidate RR Lyr which were datamined using machine learning techniques applied to the light curves of variable stars in the Palomar Transient Facility database. The observed radial velocities taken at the phase of the variable corresponding to the time of observation were converted to systemic radial velocities in the Galactic standard of rest. This only works well when the ephemerides of the variable stars are accurately known.

From our sample of 112 RR Lyr with Keck v_r we determine the radial velocity dispersion in the outer halo of the MW to be $\sim$90 km s^{-1} at 50 kpc falling to about 65 km s^{-1} near 100 kpc once a small number of major outliers are removed. The five very low $v_r(GSR)$ stars, all of which have $v_r(GSR) < -200$ km s^{-1}, are surprisingly close together on the sky at a distance of about 60 kpc, but there is no known structure at that distance in that part of the sky.

With reasonable estimates of the completeness of our sample of 447 candidates and assuming a spherical halo, we find that the stellar density in the outer halo declines as r^{-4}. Most, but not all, other recent works corroborate this functional form.

The problems we have faced have been in the accuracy of the ephemerides for the RR Lyr sample and in issues of completeness and non-RR Lyr interlopers. Further exploration of the issue of substructure in the outer halo requires a larger sample. The new Pan-STARRS RR Lyr catalog by Hernitschek et al. (2016) and by Sesar et al. (2017b) provides this, and will allow investigations which we expect to carry out in the near future to avoid most if not all of these concerns. Ultimately LSST will allow techniques similar to those we used to identify RR Lyr at even larger distances of up to several hundred kpc. Of course spectroscopic follow up of the very distant RRab we expect to find with LSST will require the next generation of extremely large telescopes beyond the current 10 m Kecks.

We are grateful to the many people who have worked to make the Keck Telescope and its instruments a reality and to operate and maintain the Keck Observatory. The authors wish to extend special thanks to those of Hawaiian ancestry on whose sacred mountain we are privileged to be guests. Without their generous hospitality, none of the observations presented herein would have been possible.

We thank the referee for helpful detailed comments that improved this paper.

This work uses data obtained with the 1.2-m Samuel Oschin Telescope at Palomar Observatory as part of the Palomar Transient Factory project, a scientific collaboration among the California Institute of Technology, Columbia University, Las Cumbres Observatory, the Lawrence Berkeley National Laboratory, the National Energy Research Scientific Computing Center, the University of Oxford, and the Weizmann Institute of Science; and the Intermediate Palomar Transient Factory project, a scientific collaboration among the California Institute of Technology, Los Alamos National Laboratory, the University of Wisconsin, Milwaukee, the Oskar Klein Center, the Weizmann Institute of Science, the TANGO Program of the University System of Taiwan, and the Kavli Institute for the Physics and Mathematics of the Universe.

The Intermediate Palomar Transient Factory project is a scientific collaboration among the California Institute of Technology, Los Alamos National Laboratory, the University of Wisconsin, Milwaukee, the Oskar Klein Center, the Weizmann Institute of Science, the TANGO Program of the University System of Taiwan, and the Kavli Institute for the Physics and Mathematics of the Universe.

The PTF database (DR3) is now publicly available at https:// www.ptf.caltech.edu/news/DR3. It includes photometry through Jan. 28, 2015.

Funding for SDSS-III has been provided by the Alfred P. Sloan Foundation, the Participating Institutions, the National Science Foundation, and the U.S. Department of Energy Office of Science. The SDSS-III web site is http://www.sdss3.org/.

SDSS-III is managed by the Astrophysical Research Consortium for the Participating Institutions of the SDSS-III Collaboration including the University of Arizona, the Brazilian Participation Group, Brookhaven National Laboratory, Carnegie Mellon University, University of Florida, the French Participation Group, the German Participation Group, Harvard University, the Instituto de Astrofisica de Canarias, the Michigan State/Notre Dame/JINA Participation Group, Johns Hopkins University, Lawrence Berkeley National Laboratory, Max Planck Institute for Astrophysics, Max Planck Institute for Extraterrestrial Physics, New Mexico State University, New York University, Ohio State University, Pennsylvania State University, University of Portsmouth, Princeton University, the Spanish Participation Group, University of Tokyo, University of Utah, Vanderbilt University, University of Virginia, University of Washington, and Yale University.

This research has made use of the NASA/IPAC Extragalactic Database (NED) which is operated by the Jet Propulsion Laboratory, California Institute of Technology, under contract with the National Aeronautics and Space Administration.

J.G.C. and B.S. thank NSF grant AST-0908139 to J.G.C for partial support during the

initial early stages of this project. S.R.B and K.H. thank the Caltech Summer Undergraduate Research Fellowship (SURF) program for support.

REFERENCES

Ahn, C. P., Alexandroff, R., Allende Prieto, C. et al., 2014, ApJS, 211, A17

Baade, W., 1926, Astron. Nach., 228, 359

Belokurov, V., Koposov, S. E., Evans, N. W. et al., 2014, MNRAS, 437, 116

Benedict, G. F., McArthur, B. E., Feast, M. W. et al., 2011, AJ, 142, 187

Bochanski, J. J., Willman, B., Caldwell, N., Sanderson, R., West, A. J., Strader, J. & Brown, W., 2014, ApJ, 790, L5

Bovy, J., Bahmanyar, A., Fritz, T. K. & Kalilvayalil, N., 2017, arXiv:1609.01298

Braga, V. F., Dall'Ora, M., Bono, G., et al., 2015, ApJ, 799, A165

Breiman, L., 2001, Machine Learning, 45, 5

Brown, W. R., Geller, M. J., Kenyon, S. J. & Diaferio, A., 2010, AJ, 139, 59

Brown, W. R., Geller, M. J. & Kenyon, S. J., 2014, ApJ, 787, A89

Carrasco, D., Barrientos, L. F., Pichara, K. et al., 2014, A&A, 584, A44

Caceres, C. & Catelan, M., 2008, ApJS, 179, 242

Chaboyer, B., 1999, in "Post-Hipparcos cosmic candles", ed. A. Heck & F. Caputo, Kluwer Academic Publishers, pg. 111

Chadid, M., Sneden, C. & Preston, G. W., 2016, arXiv:1611.02368

Cohen, J. G., 1992, ApJ, 400, 528

Cohen, J. G. & Huang, W., 2009, ApJ, 701, 1053

Cohen, J. G. & Huang, W., 2010, ApJ, 719, 931

Das, P. & Binney, J., 2016, MNRAS, 460, 1725

Deason, A. J., Belokurov, V. & Evans, N. W., 2011 MNRAS, 416, 2903

Deason, A. J., Belokurov, V., Evans, N. W. et al., 2012, MNRAS, 425, 2840

Deason, A. J., Belokurov, V., Koposov, S. E. & Rockosi, C., 2014, ApJ, 787, 30

De Propris, R., Harrison, C. D. & Mares, P. J., 2010, ApJ, 719, 1582

Dierickx, M. I. & Loeb, A., 2017, ApJ, 836, A92

Djorgovski, S. G., Drake, A. J., Mahabal, A. A. et al, 2011, in "The First Year of MAXI: Monitoring Variable X-ray Sources", ed. T. Mihara & N. Kawai, Tokyo: JAXA Special Publ. (2011)

Drake, A. J., Graham, M. J., Djorgovski, S. G. et al, 2014, ApJS, 213, 9

Faber, S., Phillips, A. C., Kibrick, R. I. et al., 2003, SPIE, 4841, 1657

Fazio, G. et al, 2004, ApJS, 154, 10

GAIA Collaboration, Brown, A. G. A.Vallenari, A. et al., 2016, arXiv:1609.04172

Grillmair, C. J., Laher, R., Surace, J. et al., 2010, ASP Conf, 434, 28

Grillmair, C. J. & Carlin, J. L., 2016, chapter in "Tidal Streams in the Local Group and Beyond", eds. H. Newberg & J. Carlin (see arXiv:1603.08936)

Hernitschek, N., Schlafly, E. .F., Sesar, B. et al., 2016, ApJ, 817, A73

Honeycutt, R. K. 1992, PASP, 104, 435

Hodapp, K. W., Kuhn, J., Thornton, R, et al., 2004, in Astrophysics & Space Science library, Vol. 300, Scientific Detectors for Astronomy, The Beginning of a New Era, ed. P. Amico, J. W. Beletic & J. E. Beletic, 501-509

Iorio, G., Belokurov, V., Erkal, D., Koposov, S. E., Nipoti, C. & Fraternali, F., 2017, MNRAS, submitted, see arXiv:1707.03833

Kafle, P. R., Sharma, S., Lewis, G. F. & Bland-Hawthorn, J., 2014, ApJ, 794, A59

Keller, S. C., Murphy, S., Prior, S., Da Costa, G. & Schmidt, B., 2008, ApJ, 678, 851

Kinman, T. D., Pier, J. R. Sunzeff, N. B., et al., 1996, AJ, 111, 1164

Kirby, E. N., Lanfranchi, A., Simon, J. D. et al, 2011, ApJ, 727, 78

Klein, C. R, Richards, J. R., Butler, N. R. & Bloom, J. S., 2014, arXiv:1402.4449

Kordopatis, G., Gilmore, G., Steinmetz, M. et al., 2013, AJ, 136, 134

Laher R. R., Surace, J., Grillmair, C. J., et al., 2014, PASP 126, 674

Law, N. M., Kulkarni, S. R., Dekany, R. G. et al., 2009, PASP, 121, 1395

Levitan, D., Fulton, B. J., Groot, P. J., et al.. 2011, ApJ, 739, 68

Longmore, A. J., Fernley, J. A. & Jameson, R. F., 1986, MNRAS, 220, 279

Longmore, A. J., Fernley, J. A. & Jameson, R. F., 1990, MNRAS, 247, 684

Madore, B. F., Hoffman, D., Freedman, W. L. et al., 2013, ApJ, 776, A135

Marconi, M., Coppola, G., Bono, G. et al, 2015, ApJ, 808, A50

McCauliff, S., Jenkins, J. M., Catanzarite, J. et al., 2015, ApJ, 806, 6

Miceli, A., Rest, A., Stubbs, C. W. et al., 2008, ApJ, 678, 865

Michalik, D., Lindegren, L. & Hobbs, D., 2015, A&A, 574, A115

Nie, J. D., Smith, M. C., Belokurov, V. et al., 2015, ApJ, 810, A153

Nikutta, R., Hunt-Walker, N., Nenkova, M., Ivezić, Z. & Elitzur, M., 2014, MNRAS, 442, 3361

Nun, I., Pichara, K., Protopapas, P. & Kim, D.-W., 2014, ApJ, 793, A23

Ofek, E. O., Frail, D. A., Breslauer, B., Kulkarni, S. R., Chandra, P., Gal-Yam, A., Kasliwal, M. M. & Gehrels, N., 2011, ApJ, 740, 65

Ofek, E. O., Laher, R., Law, N. et al., 2012, PASP, 124, 62

Rahmer, G., Smith, R., Velur, V et al., 2008, Proc. SPIE, 7014, 163

Rau, A., Kulkarni, S. R., Law, N. M. et al., 2009, PASP, 121, 1334

Richards, J. W., Starr, D. L., Butler, N. R. et al., 2011, ApJ, 733, 10

Schlafly, E. F. & Finkbeiner, D. P., 2011, ApJ, 373, A103

Schlafly, E. F., Green, G.., Finkbeiner, D. F., et al, 2014, ApJ, 789, A15

Schlegel, D., Finkbeiner, D. P. & Davis, M., 1998, ApJ, 500, 525

Sesar, B., Ivezic, A., Lupton, R. H., et al., 2007, AJ, 134, 2236

Sesar, B., Ivezić, Z., Grammer, S. H. et al., 2010, ApJ, 708, 717

Sesar, B., Jurić, M. & Ivezić, Z., 2011, ApJ, 731, A4

Sesar, B., Cohen, J. G., Levitan, D. et al., 2012, ApJ, 755, 134

Sesar, B., 2012, AJ, 144, A114

Sesar, B., Ivezić, Z., Sutart, J. et al., 2013a, AJ, 146, A21

Sesar, B., Grillmair, C. J., Cohen, J. G. et al., 2013b, ApJ, 776, 26

Sesar, B., Banholzer, S. R., Cohen, J. G. et al., 2014, ApJ, 793, A135

Sesar, B., Fouesneau, M., Price-Whelan, A., Bailer-Jones, C., Gould, A. & Rix, H.-W., 2017a, ApJ, 838, A107

Sesar, B., Hernitschek, N., Ivezic, Z. et al., 2017b, AJ, 153, 204

Sesar, B., Hernitschek, N., Dierickx, M. I. P., Fardal, M. A. & Rix, H. W., 2017, ApJ, 844, A:L4

Sharma, M., Nayak, J., Koul, M. K., Bose, S. & Mitra, A., 2014, Research in Astronomy and Astrophysics, 14, 1491

Skrutskie, M. F., Cutri, R. M., Stiening, R. et al, 2006, AJ, 131, 1163

Slater, C. T., Nidever, D. L., Munn, J. M., Bell, E. F. & Majewski, S. R., 2017, ApJ, 832, A206

Soszynski, I., Udalski, A., Szymanski, M. et al., 2016, Acta Astronomica, 66, 131

Stetson, P. B., 1996, PASP, 108, 851

Schorck, T., Christlieb, N., Cohen, J.G. et al, 2009, A&A, 507, 817

Tonry, J., L., Stubbs, C. W., Lykke, K. R. et al., 2012, ApJ, 750, A99

Torrealba, G., Catelan, M., Drake, A. J. et al, 2015, MNRAS, 446, 2251

Vivas, A. K., Zinn, R., Andrews, P., Bailyn, C. et al., 2001, ApJ, 554, L33

Werner, M. W., Roellig, T. L., Low, F. J., et al., 2004, ApJS, 154, 1

Wesselink, A. J., 1969, MNRAS, 144, 297

Wetterer, C. J. & McGraw, J. T., 1996, AJ, 112, 1046

Wright, E. L. et al, 2010, AJ, 140, 1868

Xue, X. X., Rix, H.-W., Zhao, G. et al., 2008, ApJ, 684, 1143

Xue, X. X., Rix, H. W., Yanny, B. et al., 2011, ApJ, 738, 79

Xue, X. X., Ma, Z., Rix, H.-W. et al., 2014, ApJ, 784, 170

Xue, X. X., Rix, H. W., Ma, Z. et al., 2016, ApJ, 809, A144

Yanny, B., Rockosi, C., Newberg, H. J., et al., 2009, AJ, 137, 4377

York, D. G., Adelman, J., Anderson Jr., J. E., et al., 2000, AJ, 120, 1579

Zacharias, N., Finch, C., Girard, T., et al. 2010, AJ, 139, 2184

Table 1. Light Curve Parameters for RR Lyr Candidates

RA (Deg.)	Dec (Deg.)	Period (days)	0 Phase[a] (days)	Amp (R mag)	Mean R (mag)	N(R)[b]	N(g)[c]	Quality[d]
3.77632	28.37604	0.7038231	56917.70	0.62	20.64	39	3	2
10.51398	15.64457	0.6035999	55473.75	0.70	19.94	44	131	1
13.31085	17.13101	0.6009332	55477.85	0.66	19.64	59	0	1
21.20049	20.43072	0.5733125	56239.63	0.66	20.31	82	16	1
21.39914	3.82265	0.6442016	55477.74	0.83	19.37	483	78	1
22.09602	13.81008	0.5529058	55906.68	0.58	19.12	158	0	1
26.33246	29.49091	0.5849030	56178.70	0.74	19.67	723	178	1
28.45696	20.34656	0.5965452	55430.84	0.85	19.10	500	91	1
29.46073	22.95502	0.7648931	55067.03	0.57	19.10	85	11	1
29.92910	26.09113	0.6033530	55506.60	0.58	19.11	50	0	2
32.71250	30.72719	0.5593969	55889.78	0.88	19.64	35	51	1
82.26892	3.38001	0.6566145	56974.84	0.47	19.31	48	0	1
115.18660	20.78280	0.4653525	56306.62	0.90	19.60	221	37	1
120.40829	11.03271	0.8227144	56315.70	0.49	19.87	36	0	2
125.76719	20.88205	0.6509836	55561.96	0.61	20.24	438	91	1
133.76732	63.42198	0.5425147	56225.94	0.86	19.47	69	33	1
135.73433	61.63280	0.5863690	56238.90	0.67	19.57	173	100	1
143.29643	13.29081	0.5914273	55959.91	0.70	19.46	375	138	1
153.38060	37.91186	0.6296058	56354.66	0.69	19.45	55	0	1
158.10118	6.32611	0.5824709	55953.99	0.57	19.44	35	0	2
163.17050	37.51453	0.5940006	55250.78	0.70	19.55	185	77	1
164.48911	34.74506	0.5930000	57481.68	0.70	20.22	48	45	1
180.44336	29.98856	0.6285709	56328.76	0.64	19.97	140	4	1
180.89786	32.49513	0.5869673	55297.81	0.69	20.36	174	86	1
181.01610	−2.64746	0.6868450	55615.01	1.02	20.08	65	87	1
185.11430	35.10371	0.5590766	56033.76	0.84	19.55	93	0	1
185.74637	45.19566	0.5389892	57125.90	0.94	19.98	128	131	1
188.21655	3.81825	0.6903981	55603.82	0.64	19.53	252	46	1
190.73627	39.43732	0.6328233	55984.06	0.85	20.18	83	8	1
191.65421	31.93755	0.5496644	55300.94	0.86	20.47	224	100	1

Table 1—Continued

RA (Deg.)	Dec (Deg.)	Period (days)	0 Phase[a] (days)	Amp (R mag)	Mean R (mag)	N(R)[b]	N(g)[c]	Quality[d]
193.90346	45.04369	0.5817848	55301.85	0.76	19.87	84	97	1
196.89822	27.27304	0.4651977	55663.69	0.88	20.02	596	118	1
197.85255	45.04933	0.6086488	56017.80	0.64	20.03	110	94	1
198.01382	37.50263	0.6876892	55020.68	0.65	19.67	189	33	1
198.82190	43.19382	0.5113264	55320.71	0.88	20.47	491	129	1
199.47290	32.11800	0.5893799	56342.04	0.66	19.30	468	224	1
201.59912	20.38593	0.5929822	56001.94	0.95	20.05	29	17	1
203.98247	49.90129	0.5348190	55296.00	0.89	19.75	86	0	1
204.35236	38.22820	0.5458603	55319.85	0.76	20.30	205	43	1
205.20570	36.85392	0.5540681	55275.94	0.74	20.31	102	1	1
205.90588	32.55605	0.6121942	56016.83	0.49	19.82	297	41	1
206.48932	31.08889	0.5676502	55369.63	0.96	20.30	48	19	2
207.65234	44.81257	0.6749544	56017.71	0.84	20.07	104	5	1
209.52818	37.12393	0.7011946	56330.01	0.49	20.47	285	5	1
210.14015	61.58023	0.5085552	55352.88	0.68	19.50	118	0	1
210.61269	39.29613	0.4733887	56060.90	1.00	20.64	261	53	1
210.63774	38.23235	0.6085635	55637.83	0.76	20.26	240	9	1
211.99417	36.80729	0.6083931	56035.89	0.61	20.42	103	8	2
212.58949	22.25360	0.6129632	55668.81	0.47	19.51	49	82	1
215.60762	35.91516	0.5540740	55275.94	0.63	20.18	120	13	1
216.20433	47.13657	0.5778699	56065.96	0.62	20.29	84	71	2
218.04994	40.74793	0.7578443	55279.73	0.76	20.18	192	54	1
218.17694	42.63344	0.6518604	55337.82	0.91	20.25	129	18	1
223.34651	4.97518	0.5878099	56133.73	0.68	19.53	90	5	1
223.62280	35.96528	0.5530584	56035.72	0.64	19.78	210	25	1
226.80437	25.50584	0.6792830	55360.64	0.60	20.62	64	13	3
229.78807	48.06219	0.5459260	55345.80	1.06	20.02	59	0	1
230.30850	36.28413	0.5731339	56058.84	0.82	20.05	85	11	1
231.29987	37.24485	0.6033793	56075.86	0.47	19.67	118	0	1
233.92378	36.95277	0.5269989	56039.89	0.83	20.40	97	8	1

Table 1—Continued

RA (Deg.)	Dec (Deg.)	Period (days)	0 Phase[a] (days)	Amp (R mag)	Mean R (mag)	N(R)[b]	N(g)[c]	Quality[d]
236.47386	58.07009	0.6181521	55036.85	0.90	20.18	523	180	1
239.07004	36.43287	0.5929263	55386.82	0.51	19.86	100	5	2
239.77188	38.56579	0.6242449	56039.94	0.46	20.10	140	0	1
240.32909	33.09862	0.5354092	56135.86	0.77	20.48	145	15	1
242.53758	21.51107	0.5912649	56090.65	0.73	20.27	28	1	3
242.69720	14.62067	0.5550773	55413.67	0.84	19.92	216	28	1
246.64397	6.24227	0.4882272	56003.00	0.92	19.56	68	0	1
246.97688	31.55486	0.5459153	56039.84	0.84	20.41	160	56	1
247.74931	12.76744	0.4665125	57538.67	1.01	20.53	145	0	2
248.35423	39.41171	0.5647064	55605.02	0.74	19.95	101	29	1
251.16412	38.47088	0.5246175	55702.92	0.95	19.75	231	73	1
253.12921	25.36446	0.6019734	55721.91	0.74	20.30	91	26	1
256.70535	45.84140	0.5876117	56046.88	0.63	19.65	192	36	1
257.61386	20.88444	0.5681136	55438.69	0.72	19.53	132	30	1
258.68228	34.30839	0.5655935	55407.67	0.92	19.23	166	52	1
258.77704	37.91151	0.6390487	55711.95	0.74	20.14	109	35	1
313.08780	0.13357	0.5592707	55416.69	0.78	19.95	163	66	1
318.20523	3.33563	0.6259214	55437.64	0.57	19.76	42	4	3
320.21838	6.36956	0.6970433	55467.77	0.55	19.11	59	12	2
321.29257	4.89429	0.5652243	55456.70	0.94	19.46	51	0	2
323.07294	−3.48319	0.5174600	55422.74	0.97	19.39	116	0	1
323.74008	−3.52009	0.5533006	55429.77	1.08	20.12	95	0	1
327.28622	−1.67528	0.5440798	55042.88	0.83	19.66	146	14	1
328.31757	1.61321	0.6410172	55423.82	0.87	20.17	114	19	1
329.61261	15.67164	0.5728618	55353.93	0.92	19.31	116	17	1
331.79990	15.46090	0.6015934	55498.66	0.79	19.98	141	5	1
331.87677	13.06594	0.6053543	55445.69	0.56	20.14	102	27	1
332.41092	18.24430	0.5671536	55428.81	0.61	20.31	35	16	3
332.70486	−5.19797	0.5691122	55014.77	0.98	19.72	39	30	1
332.72507	9.88418	0.5480604	55365.95	0.81	19.40	128	0	1

Table 1—Continued

RA (Deg.)	Dec (Deg.)	Period (days)	0 Phase[a] (days)	Amp (R mag)	Mean R (mag)	N(R)[b]	N(g)[c]	Quality[d]
332.92017	20.10988	0.5950155	55765.97	0.77	19.70	58	20	1
333.47647	18.46705	0.6784748	55471.69	0.78	20.24	46	20	1
334.12289	17.94743	0.5823412	55824.91	0.58	19.92	90	42	1
334.17758	23.86207	0.7038231	55482.60	0.63	20.29	99	15	1
334.32181	3.08049	0.6328018	55055.91	0.57	19.67	79	0	1
334.78058	22.16861	0.5763521	55824.82	0.54	19.69	113	19	1
334.99887	20.37570	0.5833233	55812.69	0.85	20.47	216	12	1
336.45602	14.85005	0.5597054	55123.72	0.74	19.71	124	0	1
339.64056	8.46784	0.5313083	55038.78	0.88	20.36	51	0	1
343.30026	32.76220	0.5572263	55821.73	0.85	19.73	43	80	1
344.95831	4.83823	0.7089223	55007.93	0.43	19.14	105	0	1
346.05371	8.77550	0.5578092	55426.81	0.75	20.02	70	0	2
346.24451	7.73412	0.6210057	55416.91	0.74	20.24	247	0	1
346.25085	−5.34930	0.4800212	56167.85	0.92	20.04	172	0	1
348.78879	13.35353	0.5378452	55448.79	0.96	20.05	197	0	1
349.55212	11.92246	0.5632662	56571.76	0.98	20.00	242	0	1
350.69650	33.79972	0.5440564	55142.61	0.71	19.35	309	385	1
351.98282	20.68219	0.5503856	55418.70	0.80	19.49	72	10	1
354.65012	25.68250	0.5205241	56271.65	0.98	19.10	138	89	1
355.48550	18.87469	0.6517739	55425.84	0.66	20.53	53	9	2
356.80493	3.27760	0.7114636	55038.82	0.54	19.14	59	0	1
358.89981	34.25303	0.5126550	56256.68	1.01	19.27	73	197	1
Probable	Sgr	Stream						
185.831403	11.011716	0.5416933	55899.95	0.76	···	···	···	···
189.730895	7.902692	0.4639002	55378.71	1.17	···	287	69	1
191.481527	5.967331	0.6101711	55333.68	0.55	···	280	116	1
208.767863	5.213217	0.4890867	55330.74	1.08	···	304	114	1

[a]Epoch of maximum light in heliocentric Julian date − 2400000 days. This choice, made for ease of computations, requires 7 digits in the period for accurate phasing at the present epoch.

[b]Number of epochs taken with the PTF–R filter in which the star was detected as of late 2016.

[c]Number of epochs taken with the PTF–g filter in which the star was detected as of late 2016.

[d]Observed R light curve resembles that of a RR Lyr: 1 = excellent, 2 = probable, 3 = uncertain

Table 2. v_r for RR Lyr Candidates

RA (Deg.)	Dec (Deg.)	Distance[a] (kpc)	No. Spectra	v_r[b] (GSR $km\ s^{-1}$)	$\sigma(v_r)$ ($km\ s^{-1}$)	Date
3.77632	28.37604	109.1	1	212.7	21.0	9/2015
10.51398	15.64457	75.6	1	−240.2	17.7	9/5/2016
13.31085	17.13101	65.9	1	−131.1	18.4	10/2015
21.20049	20.43073	88.3	1	−124.4	18.4	10/2015
21.39914	3.82266	59.2	1	20.4	19.7	10/2015
22.09602	13.81008	50.5	1	−21.2	17.8	10/2015
26.33246	29.49091	66.0	2	−38.0	12.9	dup[c]
28.45696	20.34657	51.2	1	−34.8	19.8	10/2015
29.46073	22.95502	54.9	1	−25.9	17.7	10/2015
29.92910	26.09113	51.7	1	23.6	17.8	10/2015
32.71250	30.72719	64.4	1	−56.5	20.0	10/2015
82.26892	3.38001	57.8	1	−42.7	17.1	9/2014
115.18660	20.78290	60.2	1	−124.7	19.3	10/2015
120.40829	11.03272	79.7	1	224.0	17.2	10/2015
125.76719	20.88206	88.6	1	−43.8	17.4	1/2014[d]
133.76732	63.42198	59.2	1	47.9	19.8	4/2016
135.73433	61.63280	63.3	2	11.6	13.1	dup
143.29643	13.29081	60.2	1	99.0	18.7	4/2016
153.38060	37.91186	61.1	1	−26.9	18.7	6/2016
158.10118	6.32611	59.4	1	−102.7	17.8	4/2016
163.17050	37.51453	62.8	1	−59.7	18.7	4/2015
164.48911	34.74506	85.5	1	−81.8	17.9	6/2016
180.44336	29.98856	77.4	1	134.3	18.3	5/2014
180.89786	32.49513	90.9	1	54.4	18.6	5/2014
181.01610	−2.64747	83.4	1	−161.8	23.4	5/2014
185.11430	35.10371	61.8	1	−29.7	19.7	4/2016
185.74637	45.19566	74.8	1	49.8	20.1	4/2016
188.21655	3.81826	64.9	1	−56.1	18.2	5/2015
190.73627	39.43733	85.4	1	26.3	19.8	5/2014
191.65421	31.93755	94.2	2	−48.6	14.0	dup

Table 2—Continued

RA (Deg.)	Dec (Deg.)	Distance[a] (kpc)	No. Spectra	v_r[b] (GSR $km\ s^{-1}$)	$\sigma(v_r)$ ($km\ s^{-1}$)	Date
193.90346	45.04369	72.3	1	−36.9	19.1	5/2014
196.89822	27.27304	72.9	1	103.6	21.8	4/2014
197.85255	45.04933	79.1	1	−88.0	18.3	5/2014
198.01382	37.50263	69.4	2	98.9	12.2	dup
198.82190	43.19382	92.1	1	29.3	20.0	4/2014
199.47290	32.11801	55.9	1	98.4	18.4	5/2015
201.59912	20.38593	79.2	1	−33.7	20.5	5/2014
203.98247	49.90129	67.1	1	56.8	20.1	5/2014
204.35236	38.22820	86.6	2	−110.9	13.5	dup
205.20570	36.85392	87.3	2	49.2	13.4	dup
205.90588	32.55605	71.8	2	108.4	12.2	dup
206.48932	31.08890	87.7	1	−19.4	20.6	7/2/2016
207.65234	44.81257	82.7	2	−73.5	15.6	dup
209.52818	37.12393	100.7	1	−11.3	17.2	4/2014
210.14015	61.58023	58.9	1	−36.4	18.6	6/2016
210.61269	39.29613	97.6	1	−38.6	23.9	4/2014
210.63774	38.23235	87.9	2	−60.9	14.8	dup
211.99417	36.80729	94.5	1	−52.3	18.1	4/2014
212.58949	22.25361	62.2	1	114.1	17.1	5/2015
215.60762	35.91516	82.4	1	56.5	18.2	4/2014
216.20433	47.13658	87.9	1	17.9	18.2	5/2014
218.04994	40.74793	89.9	1	−13.2	19.1	4/2014
218.17694	42.63344	89.1	1	−106.9	22.1	4/2014
223.34651	4.97518	62.2	1	−4.8	18.6	5/2015
223.62280	35.96528	68.6	2	15.5	12.9	dup
226.80437	25.50584	106.9	1	90.3	17.6	4/2016
229.78807	48.06219	76.2	1	−48.8	21.3	6/2016
230.30850	36.28413	78.2	1	71.8	19.6	5/2014
231.29987	37.24485	66.6	1	−3.9	17.0	6/2016
233.92378	36.95277	90.0	1	33.6	19.6	4/2016

Table 2—Continued

RA (Deg.)	Dec (Deg.)	Distance[a] (kpc)	No. Spectra	v_r[b] (GSR $km\ s^{-1}$)	$\sigma(v_r)$ ($km\ s^{-1}$)	Date
236.47386	58.07009	84.9	2	33.5	19.6	dup
239.07004	36.43287	72.4	2	−175.6	16.1	dup
239.77188	38.56579	82.3	2	64.7	12.0	dup
240.32909	33.09862	93.9	1	−38.8	19.2	4/2014
242.53758	21.51107	87.4	2	−190.2	13.4	dup
242.69720	14.62067	73.0	1	106.5	19.7	6/2016
246.64397	6.24227	59.8	1	24.3	20.3	9/5/2016
246.97688	31.55486	91.4	2	81.8	16.3	dup
247.74931	12.76744	92.3	1	171.1	21.0	5/2014
248.35423	39.41171	74.7	1	46.9	21.5	4/2014
251.16412	38.47088	66.5	1	−152.3	20.5	5/2014
253.12921	25.36446	89.2	2	82.9	13.4	dup
256.70535	45.84146	65.5	1	52.8	18.2	9/2015
257.61386	20.88444	61.7	2	−46.0	13.3	dup
258.68228	34.30840	53.6	1	88.9	20.3	9/2015
258.77704	37.91151	84.2	2	−83.1	13.4	dup
313.08780	0.13357	74.5	1	−27.6	19.3	9/2014
318.20523	3.33564	70.3	1	97.6	17.7	9/2014
320.21838	6.36956	53.7	1	−34.6	17.6	10/2015
321.29257	4.89429	59.6	2	−118.8	14.4	dup
323.07294	−3.48319	56.1	2	10.2	14.6	dup
323.74008	−3.52009	80.2	1	−98.3	21.4	10/2015
327.28622	−1.67528	64.7	1	45.3	19.6	9/5/2016
328.31757	1.61321	85.7	1	−21.5	18.4	9/2014
329.61261	15.67164	55.7	2	−210.9	14.4	dup
331.79990	15.46091	76.9	1	26.6	19.4	10/2015
331.87677	13.06594	82.8	1	−106.4	17.7	9/2014
332.41092	18.24431	88.1	2	−72.6	12.8	dup
332.70486	−5.19797	67.3	1	141.8	20.7	9/2014
332.72507	9.88418	57.4	1	−256.2	19.5	10/2015

Table 2—Continued

RA (Deg.)	Dec (Deg.)	Distance[a] (kpc)	No. Spectra	v_r[b] (GSR $km\ s^{-1}$)	$\sigma(v_r)$ ($km\ s^{-1}$)	Date
332.92017	20.10989	67.4	1	94.4	19.2	10/2015
333.47647	18.46705	89.7	1	−155.1	19.3	9/2014
334.12289	17.94743	74.1	1	83.2	17.8	9/5/2016
334.17758	23.86207	92.7	1	37.1	18.2	9/5/2016
334.32181	3.08049	67.5	1	−162.4	17.8	9/2014
334.78058	22.16861	66.5	1	−101.6	17.5	9/5/2016
334.99887	20.37570	95.7	1	60.8	19.8	10/2015
336.45602	14.85005	66.6	1	−238.2	19.0	9/2014
339.64056	8.46785	88.5	1	15.5	20.0	10/2015
343.30026	32.76222	67.1	1	57.1	19.8	10/2015
344.95831	4.83823	54.7	1	−237.4	16.8	10/2015
346.05371	8.77550	76.8	1	79.8	19.1	10/2015
346.24451	7.73412	87.6	1	−150.4	19.0	9/5/2016
346.25085	−5.34935	74.4	1	−88.8	20.3	10/2015
348.78879	13.35353	77.1	1	−178.3	20.5	6/2016
349.55212	11.92246	76.2	1	−75.5	20.8	6/2016
350.69650	33.79972	56.1	1	−25.8	18.8	10/2015
351.98282	20.68220	59.8	1	−135.7	19.4	10/2015
354.65012	25.68251	50.0	1	−106.3	20.8	10/2015
355.48550	18.87470	101.4	1	100.8	18.4	9/5/2016
356.80493	3.27760	54.6	1	−7.6	17.5	9/5/2016
358.89981	34.25304	53.1	1	−55.9	20.9	10/2015
Sgr	Stream ?					
185.831403	11.011716	86.9	1	−62.5	20.5	4/2014
189.730895	7.90269	86.1	1	−120.2	25.5	4/2014
191.481527	5.967331	79.5	1	4.1	19.2	5/2014
208.767863	5.213217	83.9	1	−16.4	29.0	4/2014

[a]Heliocentric distance.

[b]v_r corrected to the systemic velocity, then to the heliocentric velocity, and then to the Galactic system of rest.

[c]Two Keck/Deimos spectra have been taken. See Table 3 for details.

[d]A DBSP spectrum taken with the Hale Telescope at Palomar Observatory.

Table 3. v_r for RR Lyr Candidates With Two Keck Deimos Spectra

RA	Dec (2000)	v_r[a] (GSR: $km\ s^{-1}$)	$\sigma(v_r)$[b] ($km\ s^{-1}$)	Date
Same night				
135.734329	61.632797	−1.6	18.5	4/5/2016
		24.7	18.5	4/5/2016
204.352357	38.228202	−111.6	19.1	4/5/2016
		−110.3	19.1	4/5/2016
205.905884	32.5560532	109.1	17.2	4/30/2014
		107.7	17.2	4/30/2014
323.072937	−3.48319101	−6.0	20.6	10/14/2015
		26.5	20.6	10/14/2015
329.612610	15.671644	−217.9	20.3	10/13/2015
		−203.9	20.3	10/13/2015
332.410919	18.2443104	−67.6	18.1	10/13/2015
		−77.5	18.1	10/13/2015
Consecutive	Nights			
198.013824	37.5026283	109.1	17.2	4/30/2014
		88.7	17.6	5/1/2014
205.205704	36.8539162	47.3	19.0	4/30/2014
		51.0	19.1	5/1/2014
207.652344	44.8125725	−89.9	22.1	4/30/2014
		−57.1	21.0	5/1/2014
239.070038	36.4328651	−181.5	22.7	4/30/2014
		−169.8	19.7	5/1/2014
246.976883	31.5548630	84.4	23.0	4/30/2014
		79.2	23.2	5/1/2014
∼1 Month Apart				
26.332462	29.490912	−43.3	18.2	9/19/2015
		−32.8	19.0	10/11/2015

Table 3—Continued

RA	Dec (2000)	v_r[a] (GSR: $km\ s^{-1}$)	$\sigma(v_r)$[b] ($km\ s^{-1}$)	Date
242.537582	21.5110741	−183.8	18.9	6/2016
		−196.6	18.9	7/2016
258.777034	37.911508	−94.1	20.0	6/2016
		−72.1	20.0	9/5/2016
Nights Separated By	A Year or More			
191.654206	31.937550	−22.8	19.8	4/30/2016
		−74.3	23.0	5/29/2014
210.637741	38.2323532	−55.3	20.9	4/30/2014
		−66.6	19.1	4/5/2016
223.622803	35.9652824	25.4	18.3	5/18/2014
		5.6	18.3	6/4/2016
236.473862	58.0700874	20.7	27.7	4/30/2014
		46.2	20.2	6/4/2016
239.771881	38.5657883	48.9	17.0	5/28/2014
		80.5	17.0	6/4/2016
253.129211	25.3644562	78.2	19.0	4/30/2014
		87.7	19.0	6/4/2016
257.613861	20.8844376	−65.0	18.8	9/2015
		−27.0	18.8	4/2016
321.292572	4.89428520	−140.7	20.4	10/2015
		−96.9	20.4	7/2016

[a]v_r corrected to the systemic velocity, then to the heliocentric velocity, and then to the Galactic system of rest.

[b]The 1σ uncertainty in the GSR radial velocity.

Table 4. RR Lyr Candidates That Are Not RR Lyr(ab)[a]

RA	Dec	PTF−R	Comments
QSO	(not in NED	as of 7/2016)	
3.776320	28.376036	20.6	broad em. 5650 Å
22.518406	5.325709	20.1	broad em. 6200, 9200 Å
67.040609	0.551808	19.9	broad em. 6600 Å
328.276107	10.135809	20.0	broad em. 5450 Å
338.817911	8.405663	20.3	broad em. 6850 Å
Variable	Stars		
211.637100	20.845664	19.9	variable
241.766698	22.951423	19.8	variable, period 0.2278 days.
250.411946	39.1151	20.2	variable
291.426967	38.535437	20.3	variable
341.865780	27.500455	20.5	RRc ? period 0.336 days
344.190408	−5.472125	19.7	SX Phe period 0.0402351 days
355.394934	13.261791	19.8	RRc period 0.423 days

[a]Objects which are not *ab* type RR Lyr based on their Deimos spectra or on the period derived from their PTF light curves.

Table 5. Characteristics Of The v_r Distribution

r Range	N	$< v_r(sys) >$[a] $(km\ s^{-1})$	σ[b] $(km\ s^{-1})$[b]
All			
$50 < r < 70$	51	-27.4	97.4 (95.3)
$70 < r < 85$	35	-25.0	103.5 (101.5)
$50 < r < 85$	86	-26.2	99.4 (97.4)
$85 < r < 106$	26	6.2	91.9 (89.7)
– Outliers[c]			
$50 < r < 70$	47	-9.3	78.7 (76.1)
$70 < r < 85$	33	-26.0	89.4 (87.1)
$50 < r < 85$	80	-16.2	83.1 (80.7)
$85 < r < 109$	23	-1.35	68.0 (65.0)

[a]All velocities are in the Galactic standard of rest.

[b]The σ values are followed by values in parentheses which have a measurement uncertainty of 20 $km\ s^{-1}$ removed in quadrature.

[c]Outliers are defined as: $|v_r| > 170\ km\ s^{-1}$ for $r > 85$ kpc, $> 200\ km\ s^{-1}$ for $50 < r < 85$ kpc.

Table 6. Fraction of Candidate RR Lyr That Have Been Confirmed

r Range (kpc)	N(RR Lyr) Confirmed RR Lyr with v_r[b]	N(RR Lyr) $Pr > 0.8$ PTF Candidates	Fraction[a] (Confirmed/Candidates)
$50 < r < 64$	33	155	0.21
$64 < r < 78$	38	86	0.44
$78 < r < 85$	15	30	0.50
$85 < r < 92$	14	25	0.56
$92 < r < 99$	9	16	0.56
$r > 99$	3	8	0.38

[a]The ratio of the number of candidate RR Lyr selected from the PTF database in 2014 with $Pr > 0.8$ to those from this sample with Keck/Deimos v_r for each distance bin.

[b]The number of RR Lyr in this distance bin from the PTF sample that have been confirmed with Keck/Deimos spectroscopy and have a v_r given in Table 2.

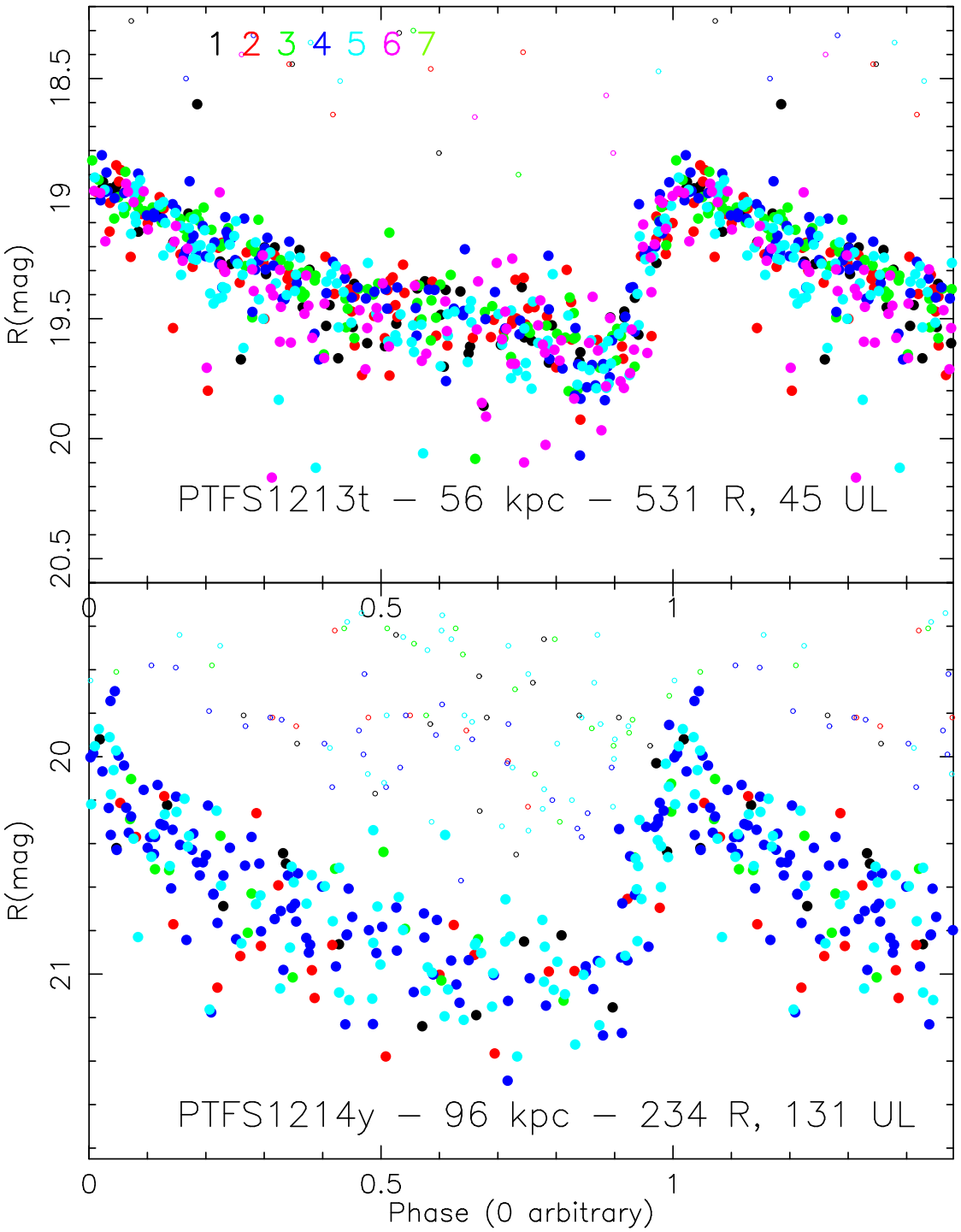

Fig. 1.— Phased light curve for PTFS1213t (RA, Dec: 199.472902 32.118009, $r = 56$ kpc, 576 epochs of R imaging, of which 45 are only upper limits, indicated by small open circles) and for PTF1214y (RA, Dec: 210.61273 39.29614, $r = 96$ kpc, 365 epochs of R imaging, of which 131 are only upper limits). The colors denote the years since the first PTF observation; the key for the colors is at the top of the upper panel, black points from the first year, etc.

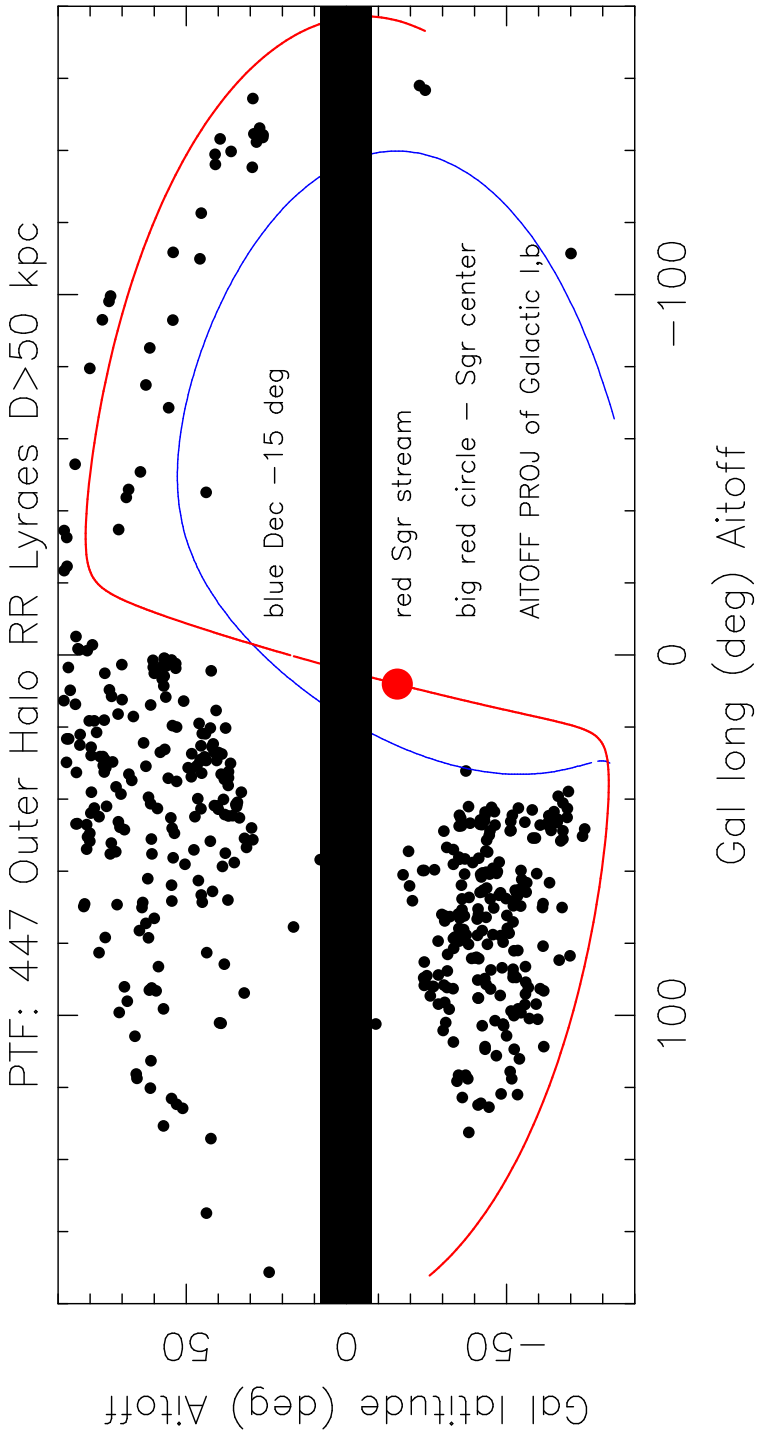

Fig. 2.— The location on the sky in an Aitoff projection of galactic coordinates of the sample of 447 PTF outer halo candidate RR Lyr stars. The larger points have distances beyond 85 kpc. The locus of the Sgr stream is denoted by the red curve. The center of the Sgr galaxy is indicated by the large red dot. Dec −15 deg is indicated by the blue curve.

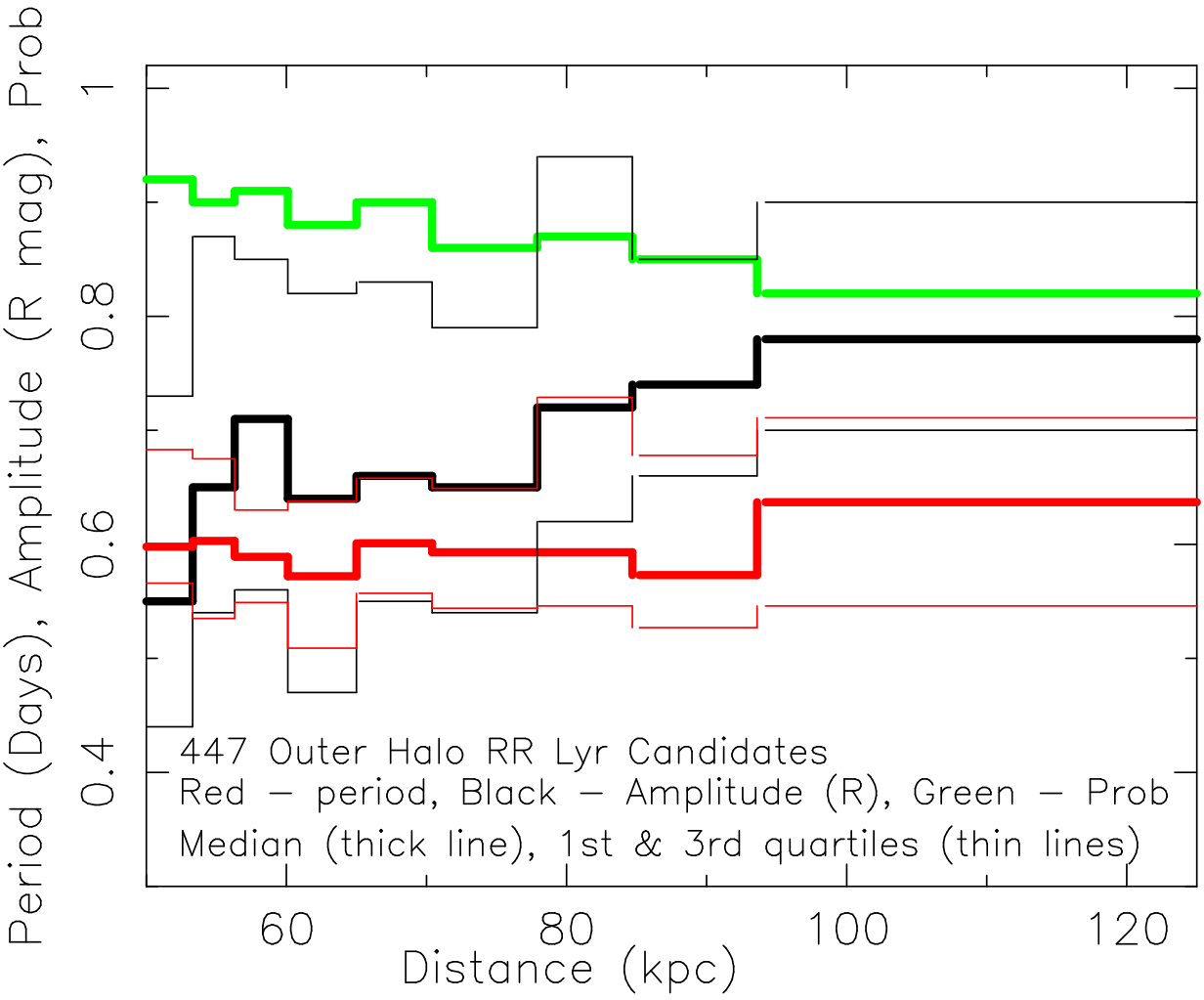

Fig. 3.— Median, first, and third quartiles of periods and of amplitudes of our sample of 447 RR Lyr candidates beyond 50 kpc are shown in 9 distance bins. The median probability is also shown for each bin. The first bin contains 47 RR Lyr, while the more distant ones each contain 50 variables.

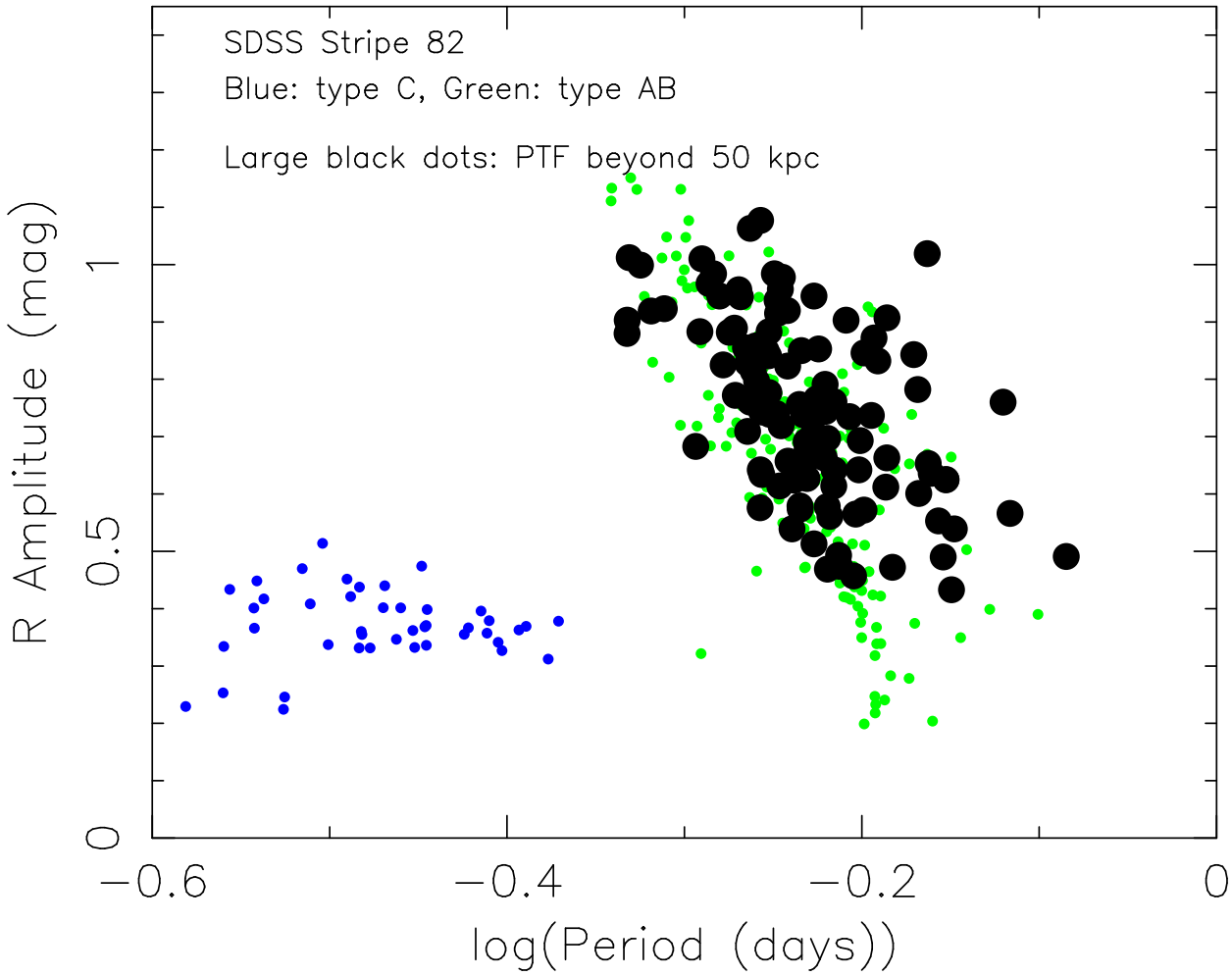

Fig. 4.— The period – amplitude relation for the 112 Keck PTF outer halo RR Lyr stars is shown (large black points), as well as that of the SDSS Stripe 82 sample from Sesar et al. (2010) (type *ab* in green, type *c* in blue).

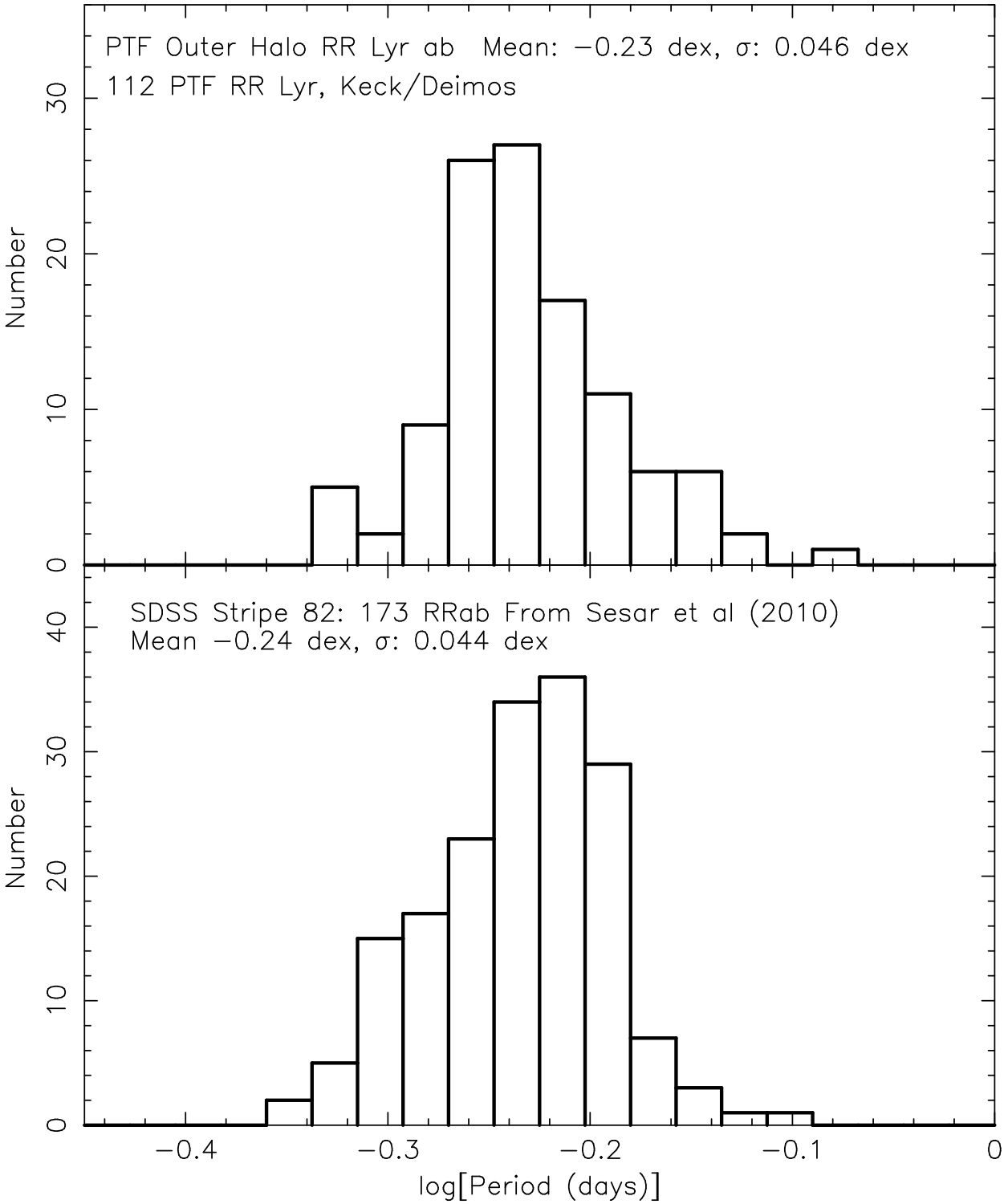

Fig. 5.— The histogram of log(period) for our Keck v_r sample is shown in the upper panel, while that of the 173 RR Lyr *ab* from Sesar et al. (2010) is shown in the lower panel.

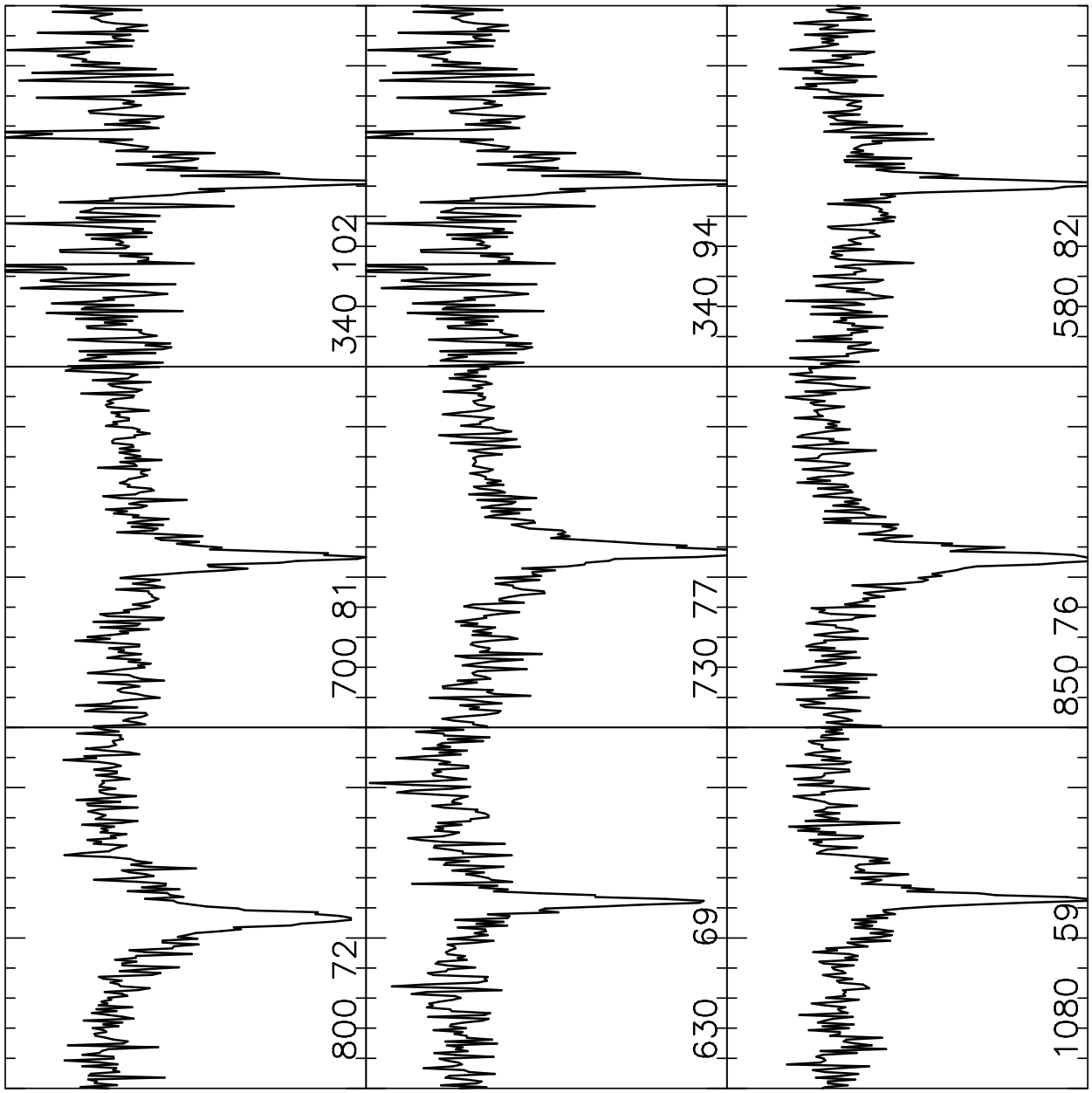

Fig. 6.— Plots of the 1D extracted spectra for 9 RR Lyr from our sample. The vertical scale of each panel ranges from 1.2 times the continuum signal near Hα to 0.5 times the continuum signal. The text at the bottom of each panel gives the continuum signal level and the distance. The panels are ordered by the distance from 59 (bottom left) to 102 kpc (upper right). The wavelength range (X axis) of each panel is 6500 to 6620 Å.

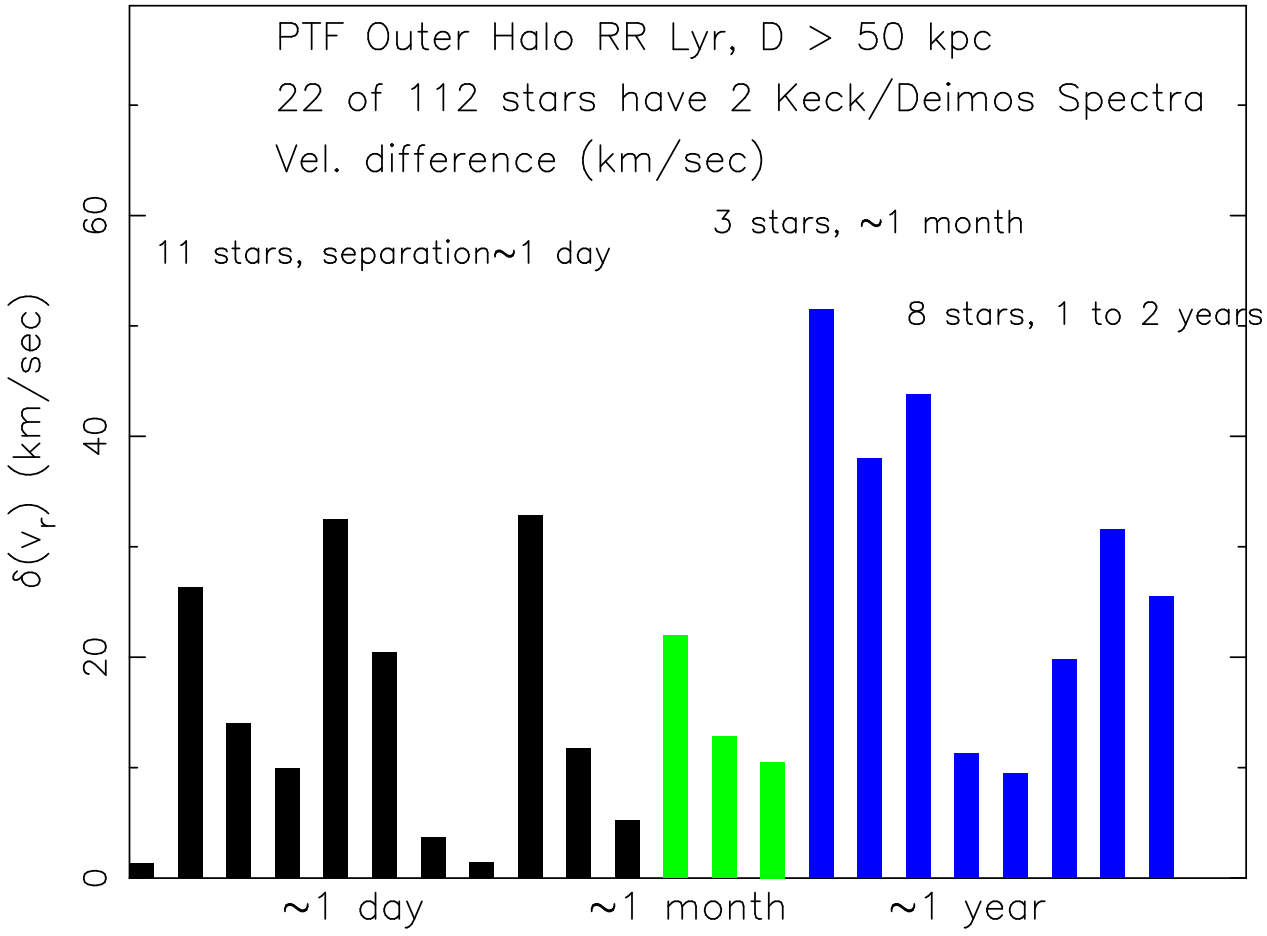

Fig. 7.— The sample of 22 stars with two Keck/Deimos spectra is shown. The vertical axis is the absolute value of the difference in $v_r(GSR)$ for each star with more than one spectrum. The horizontal axis sorts the pairs in order of increasing separation in time between the two observations, with difference ranging from ~1 day to ~1 year.

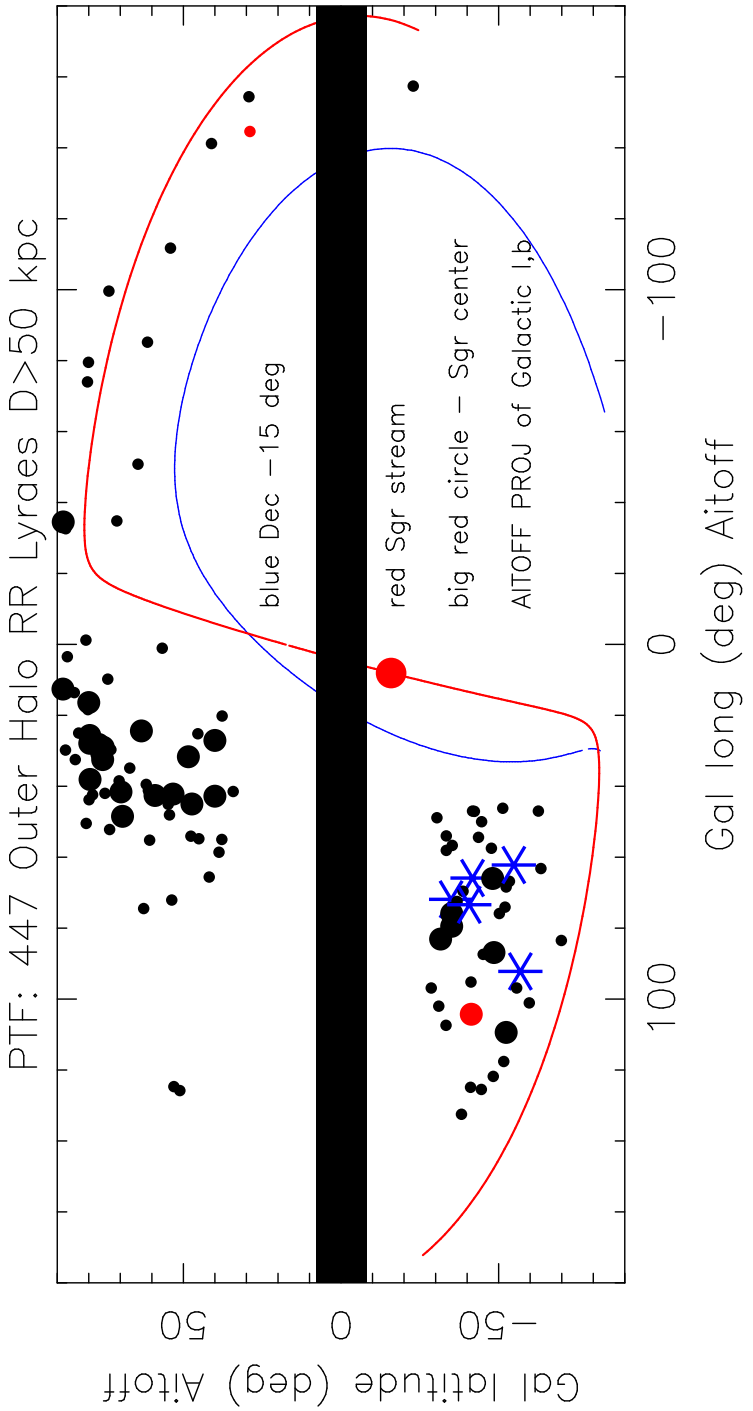

Fig. 8.— The location on the sky in galactic coordinates of the PTF outer halo RR Lyr stars with v_r from Keck/Deimos is shown in an Aitoff projection of Galactic coordinates. The larger dots denote RR Lyr with distances beyond 85 kpc. The five large blue stars indicate the only stars of the sample of 116 which have $v_r(GSR) < -200$ km/sec, while the red points have $v_r(GSR) > 200$ km/sec. The area around the Galactic plane that was excluded is indicated by the solid bar. The locus of the Sgr stream is denoted by the red curve, with the nucleus of the Sgr dwarf galaxy indicated by the large red circle. Dec −15 deg is indicated by the blue curve.

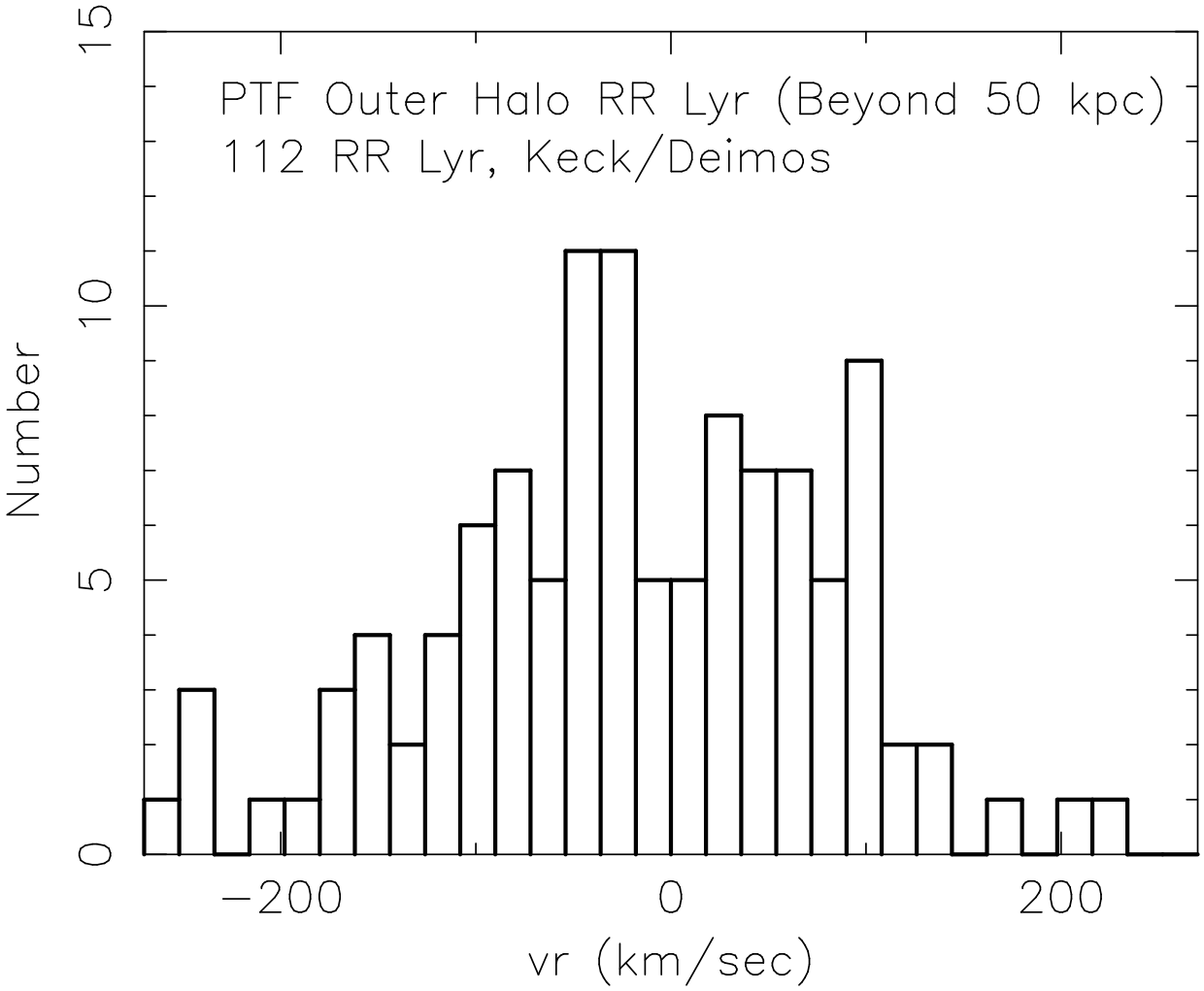

Fig. 9.— A histogram of the Keck/Deimos v_r for the sample of 112 RR Lyr in the outer halo of the Milky Way beyond 50 kpc.

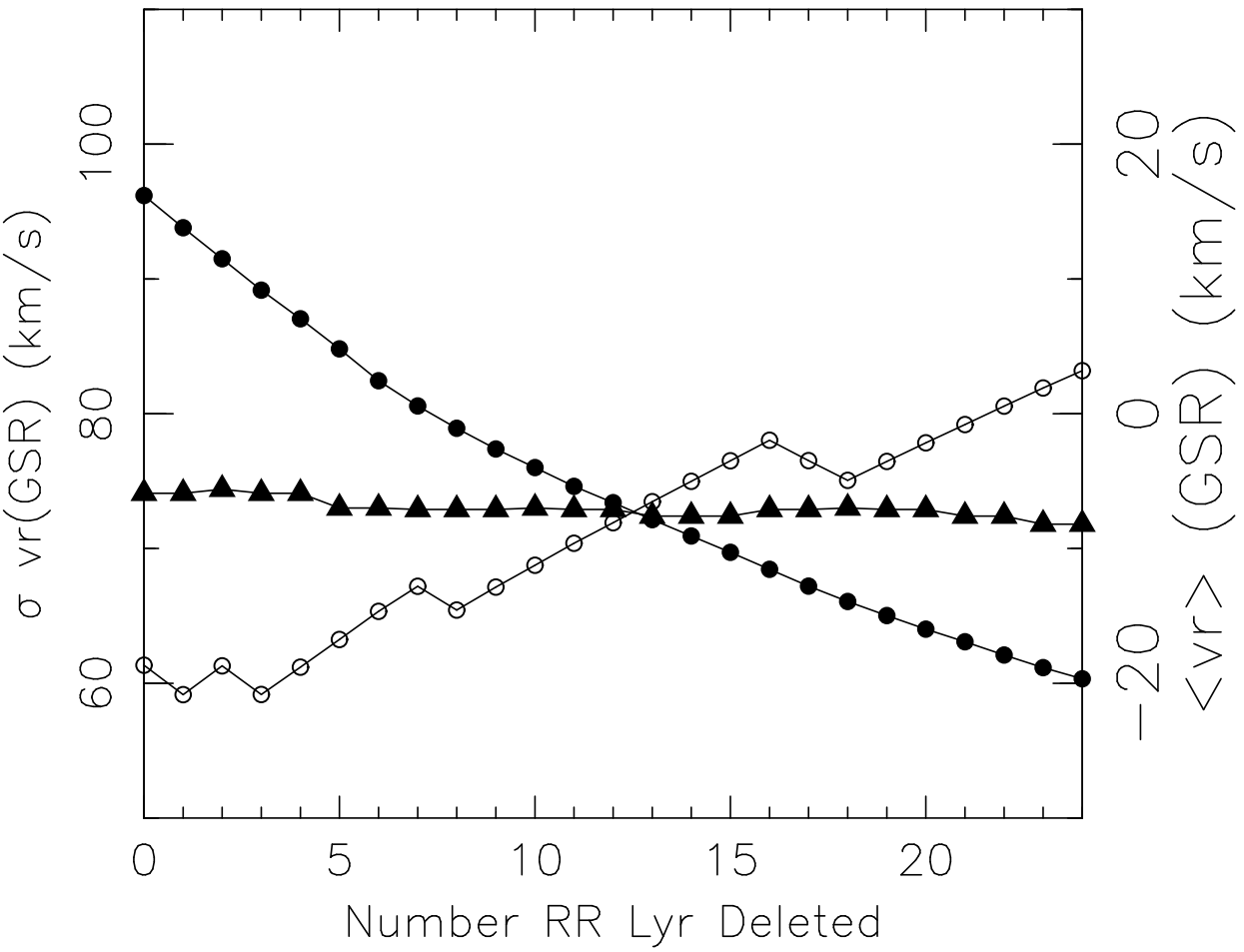

Fig. 10.— Tests sequentially deleting the largest outlier in $|(v_r - < v_r >)|$ where the mean v_r is that of the previous iteration are shown for $\sigma(v_r)$ as filled circles, as filled triangles for the median distance, and as open circles for the median distance of our RRab sample in the outer halo. The left axis gives the vertical scale for $\sigma(v_r)$, while the right axis gives the vertical scale for the other two curves.

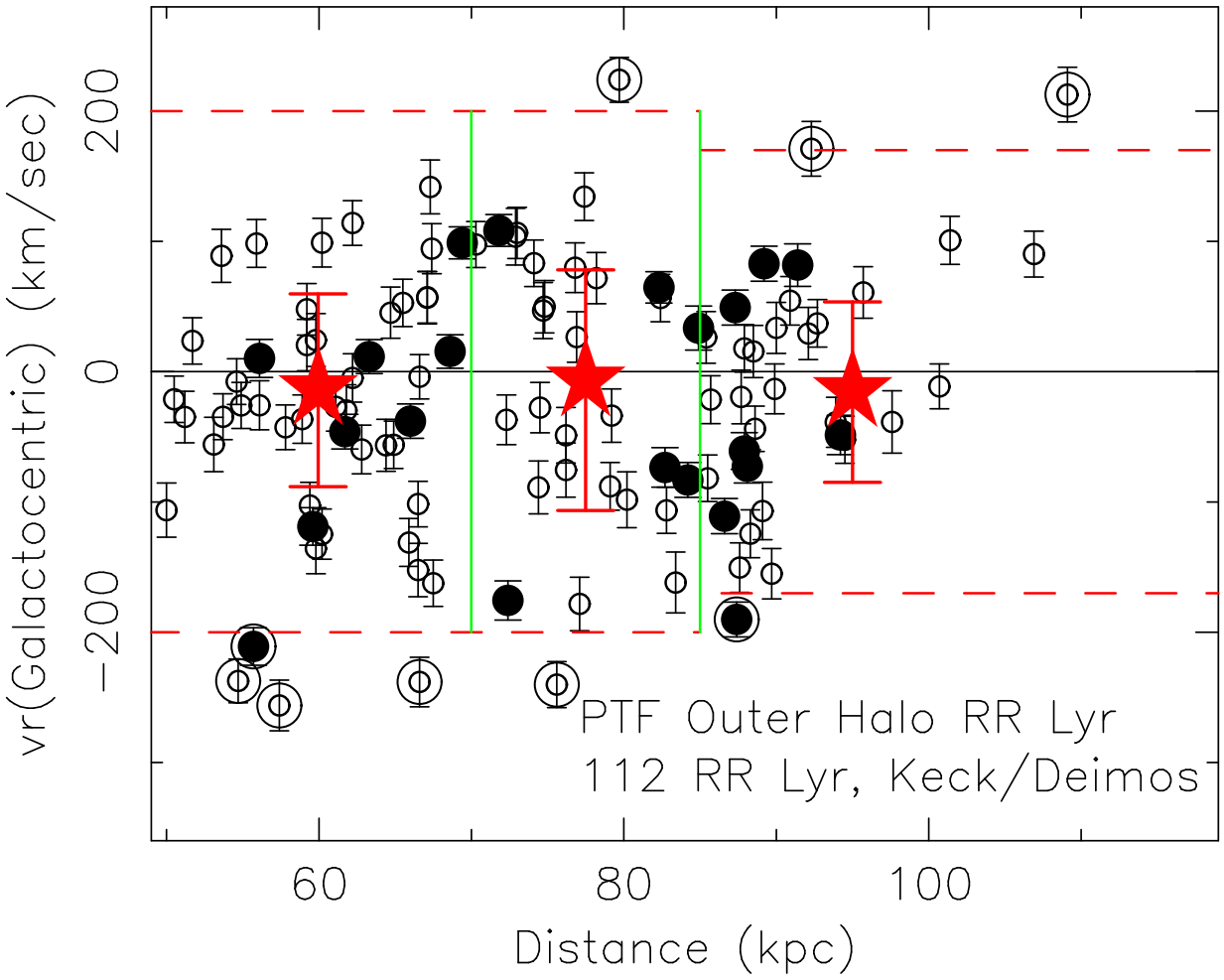

Fig. 11.— Radial velocities in the galactic standard of rest are shown as a function of distances for our sample of 112 RR Lyr selected from the PTF with Keck/Deimos moderate resolution spectra. Filled circles denote stars with two Deimos spectra, open circles have one spectrum. 1σ error bars are shown for each RR Lyr. The regions (both for high and for low v_r) considered outliers in v_r are indicated by the dashed horizontal lines. The two vertical lines denote the boundaries between the close, middle, and far samples. The large stars are located at the median distance for each of these three samples in X, at the mean $v_r(GSR)$ in Y, and their error bars indicate the velocity dispersion for each of the three distance groups ignoring the outliers. The 9 outliers are circled. See Table 5 for detailed statistics of the $v_r(GSR)$ distribution.

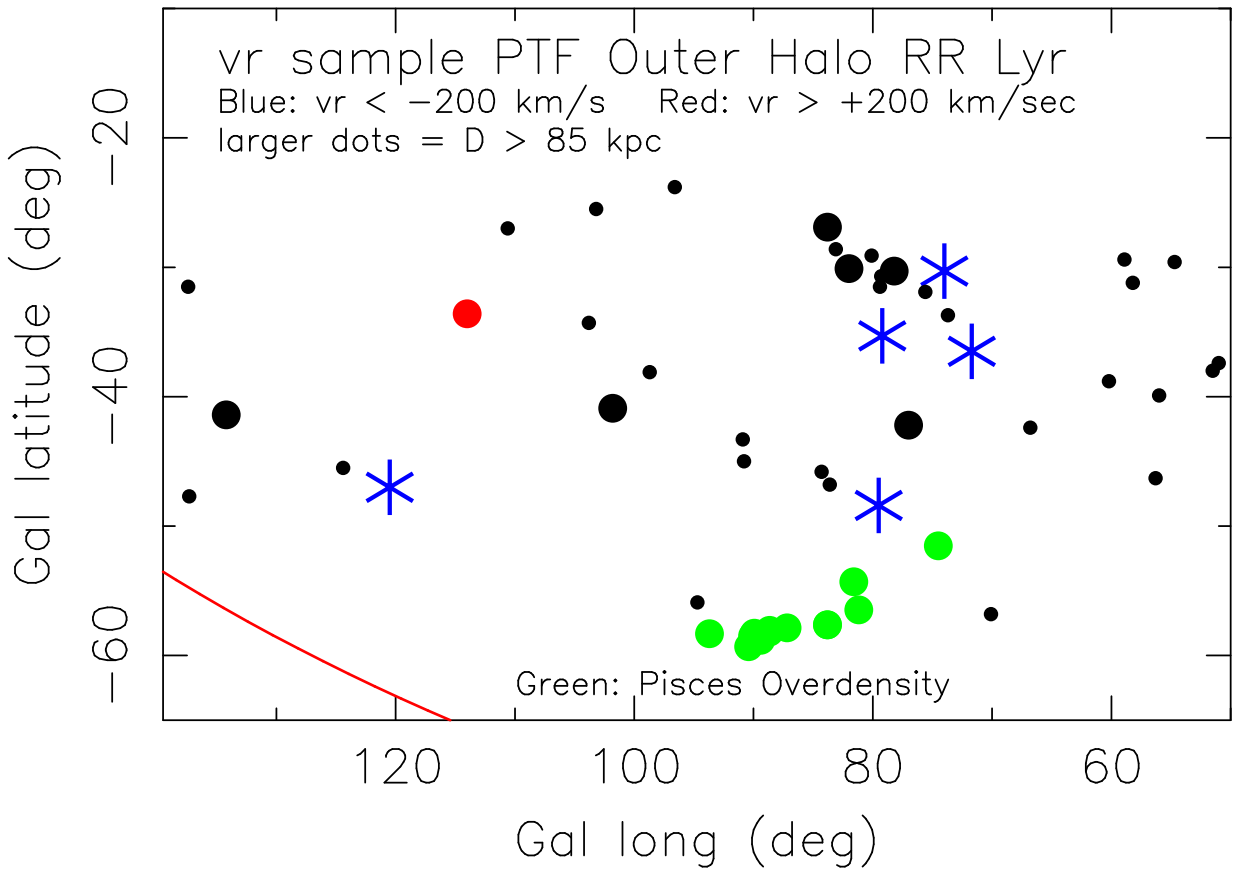

Fig. 12.— The v_r sample is shown in a plot of Galactic coordinates for a small subset of the total area on the sky covered. All the candidates with $v_r < -200$ km/sec, indicated as large blue stars, lie within this small area on the sky. The location of the RR Lyr in the Pisces overdensity found by Sesar et al. (2007) is shown in green. The red curve denotes the Sgr stream.

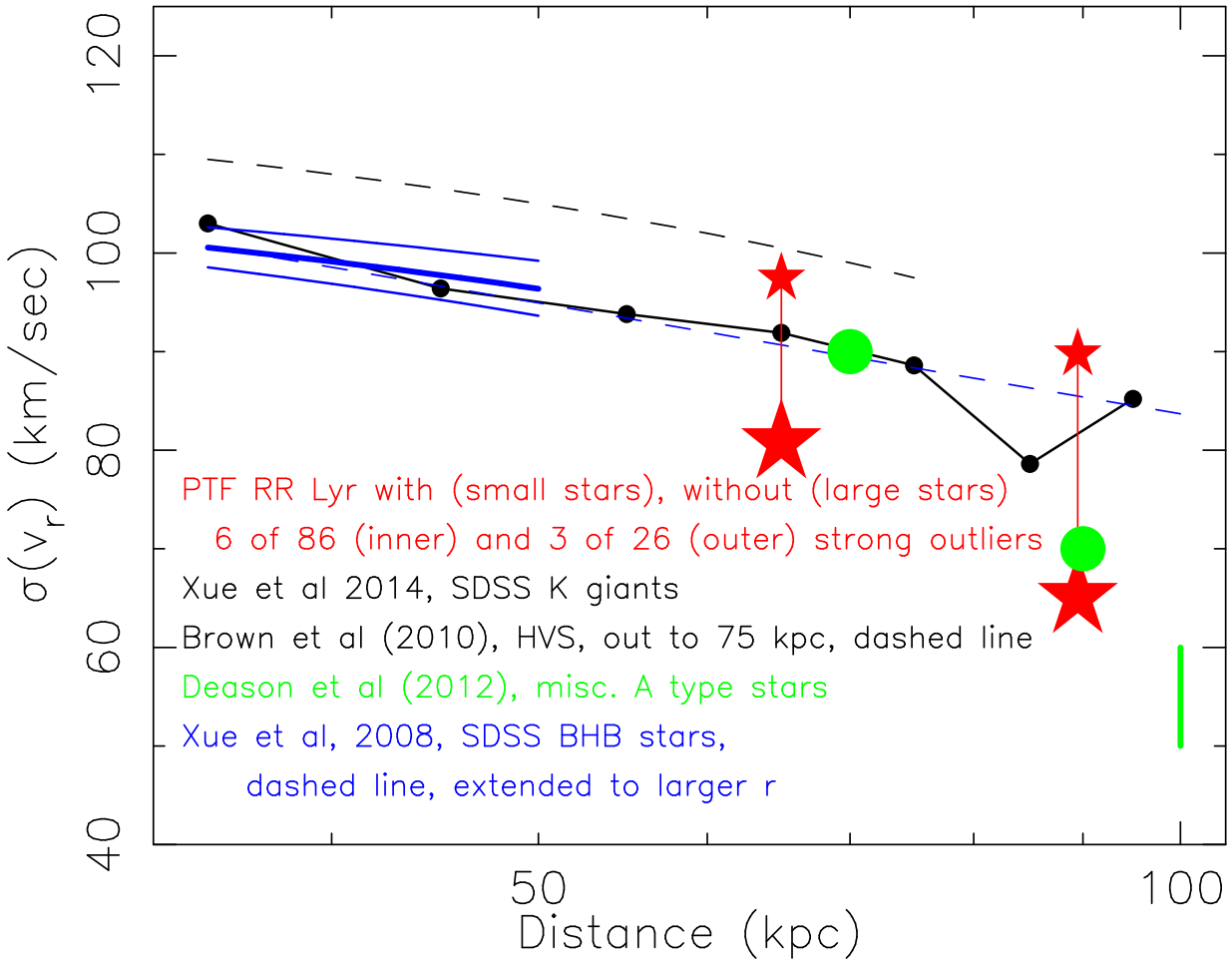

Fig. 13.— $\sigma(v_r)$ in the Galactocentric rest frame are shown for our inner and outer sample of RRab from the PTF (split at 85 kpc), with (large red stars) and without (smaller red stars) eliminating the strong outliers (3 in the outer sample, and 8 in the inner sample). Values that have been derived in several recent studies by Xue et al. (2008), whose extrapolation to larger r is indicated by a dashed line, Xue et al. (2014), Brown, Geller & Kenyon (2014), and Deason et al. (2012) are also indicated. Note that the X-axis has a logarithmic scale.

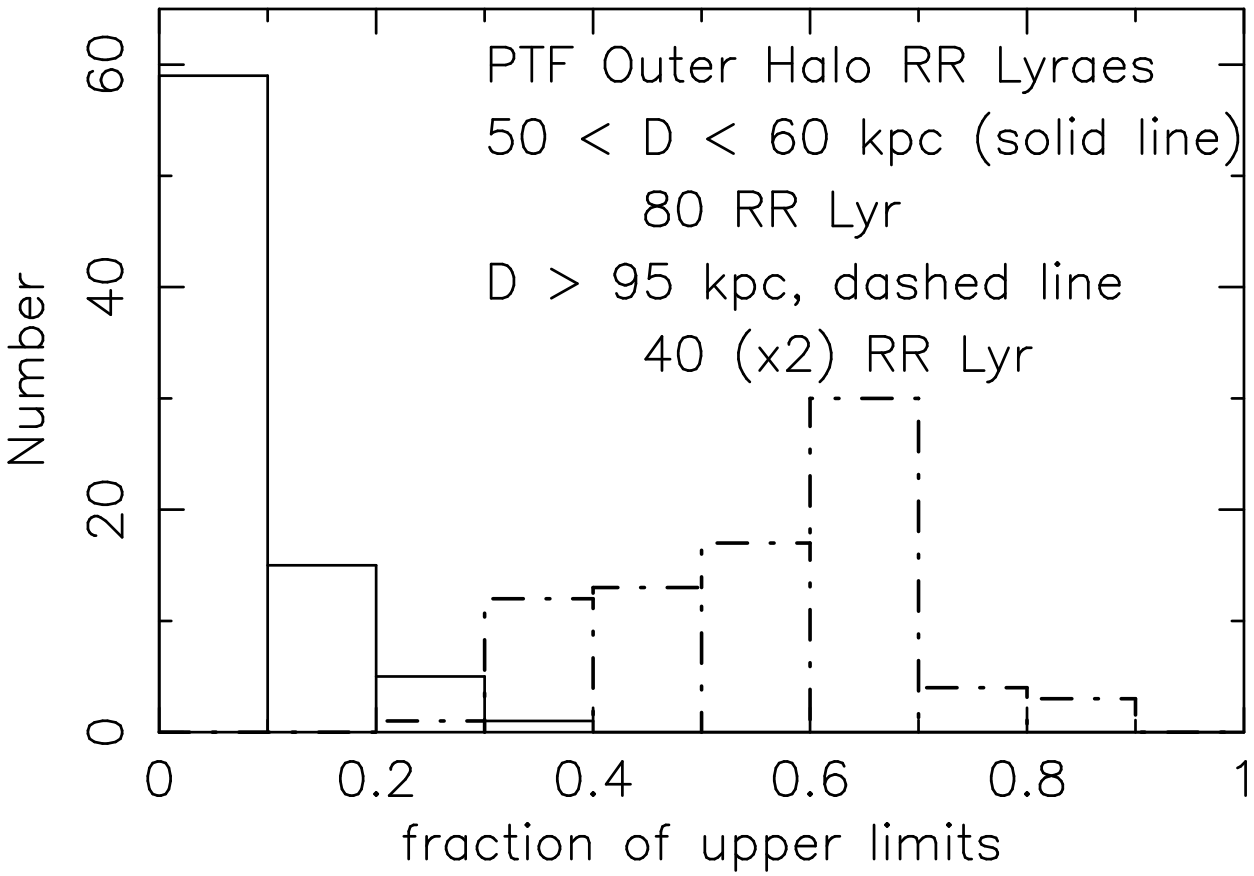

Fig. 14.— Fraction of upper limits among the total observed epochs of the PTF are shown for samples of candidate RR Lyr with distances ∼55 kpc vs those with distances > 95 kpc. For the most distant RRab, a much larger fraction of the PTF images do not result in a detection of the candidate RR Lyr.

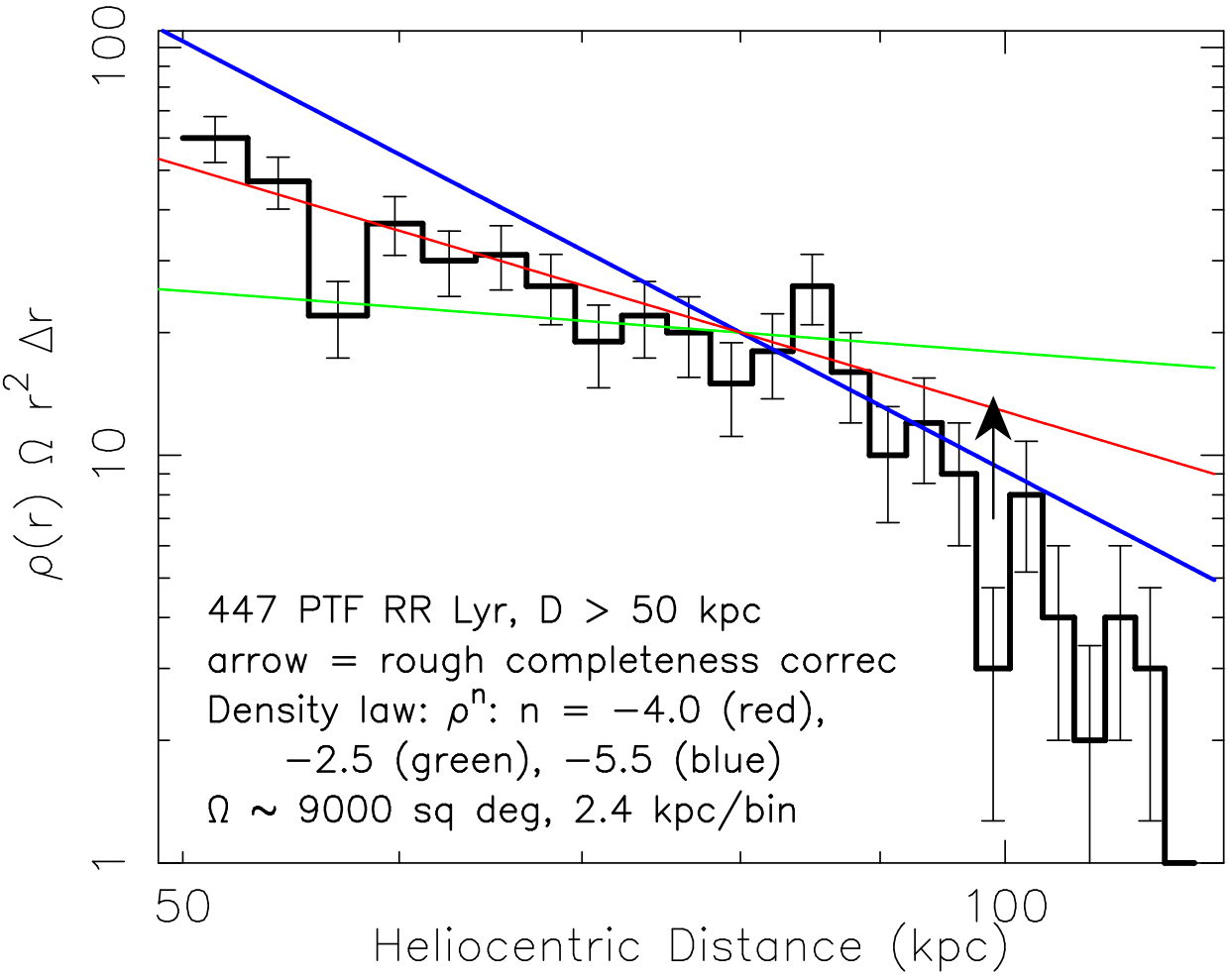

Fig. 15.— Histogram with distance of the 447 candidate RR Lyr stars from the PTF sample beyond 50 kpc. Power laws for $n = -2.5$, -4.0, and -5.5 are shown. The data are reasonably well fit for $n \sim -4$ out to ∼90 kpc, after which a steeper slope is seen. However at that distance, the incompleteness effects are severe; a guess at the minimum completeness correction at such distances is shown by the upward pointing arrow.